https://doi.org/10.5194/egusphere-2025-4190
Preprint. Discussion started: 4 October 2025

Assessment of transparent exopolymer particles in the Arctic Ocean implemented into the coupled ocean–sea ice–biogeochemistry model FESOM2.1–REcoM3

Moritz Zeising[1], Laurent Oziel[1], Silke Thoms[1], Özgür Gürses[1], Judith Hauck[1,2], Bernd Heinold[3], Svetlana N. Losa[1,4], Manuela van Pinxteren[3], Christoph Völker[1], Sebastian Zeppenfeld[3], and Astrid Bracher[1,5]

[1]Alfred Wegener Institute Helmholtz Center for Polar and Marine Research, Bremerhaven, Germany
[2]University of Bremen, Bremen, Germany
[3]Leibniz Institute for Tropospheric Research, Leipzig, Germany
[4]Shirshov Institute of Oceanology, Russian Academy of Sciences, Moscow, Russia
[5]Institute of Environmental Physics, University of Bremen, Bremen, Germany

Correspondence: Moritz Zeising (moritz.zeising@awi.de)

Abstract. We present an assessment of the coupled ocean–sea ice–biogeochemistry model FESOM2.1–REcoM3, in which we integrated state equations for dissolved acidic polysaccharides (PCHO) and transparent exopolymer particles (TEP), as proposed by Engel et al. (2004), to explicitly describe these two organic carbon pools in the Arctic Ocean. PCHO is simulated as one fraction of the phytoplankton exudates, which can then aggregate to form larger particles, TEP. Since observational datasets on TEP are rare in time and space, we systematically assess the novel model implementation by stepwise discussing the essential components of the organic carbon cycle. Firstly, the simulated phytoplankton biomass yields good results when compared to in situ and remote-sensing products of total Chlorophyll *a* and particulate organic carbon. Secondly, we compare PCHO to observations in the Fram Strait, as an exemplary data-rich region, and to datasets in other regions of the Arctic Ocean. The model realistically reproduces a high phytoplankton exudation rate of PCHO under nutrient-depleted conditions. Thirdly, we assess simulated TEP concentrations by comparing them to in situ measurements from several campaigns to the Arctic Ocean. The simulation provides a first estimate of mean TEP concentrations of 200–400 $\mu g\,C\,L^{-1}$ on the continental shelves and 10–50 $\mu g\,C\,L^{-1}$ in the central basins (0–30 m depth range). Lastly, we put the model performance into a global context for TEP concentrations in the upper ocean layer. As such, the implementation of PCHO exudation, aggregation to TEP, and their remineralization processes into FESOM2.1–REcoM3 offers a reasonably good agreement with observations, on which further modeling work can build upon.

1 Introduction

The global ocean contains a vast amount of dissolved organic carbon (DOC, 662 $Pg\,C$; Hansell et al., 2009), the characteristics and dynamics of which are not yet fully understood (Arnosti et al., 2021; Hansell et al., 2009; Hansell and Orellana, 2021; Hansell et al., 2024; Ogawa and Tanoue, 2003; Repeta and Aluwihare, 2024). Marine organic carbon forms a continuum rang-

https://doi.org/10.5194/egusphere-2025-4190
Preprint. Discussion started: 4 October 2025

ing from low-molecular weight compounds over humic- and gel-like structures of varying sizes to sinking particles, which all include carbohydrate, lipid, and proteinaceous compounds (Ogawa and Tanoue, 2003). Out of practicality, this continuum is often operationally divided into particulate and dissolved organic carbon pools based on filtration (POC, DOC, respectively; Repeta and Aluwihare, 2024). Polysaccharides comprise a significant portion of the carbohydrate pool in the ocean (Arnosti et al., 2021; Ogawa and Tanoue, 2003; Pakulski and Benner, 1994), and often contain acidic functional groups or moieties (Krembs and Deming, 2008; Passow, 2002; Zhou et al., 1998). Dissolved acidic polysaccharides (PCHO) can form complex networks which are referred to as marine gels (Engel et al., 2020; Verdugo et al., 2004). These polysaccharides are produced by phytoplankton as anti-freezing agents (Krembs and Deming, 2008), against salinity stress (Steele et al., 2014), or as exudation products in response to nutrient stress, a process referred to as carbon overconsumption or carbon overflow (Engel et al., 2004, 2020; Toggweiler, 1993), or even by bacteria (Wurl et al., 2011). We use "exudation" here as a general term that encompasses both the active and regulated excretion (Chin et al., 2004) as well as the passive release of organic carbon (especially when the cells are in non-healthy physiological condition; Thornton, 2014).

PCHO contributes to the formation of transparent exopolymer particles (TEP), which are operationally defined as particles larger than 0.4 µm that can be stained by Alcian Blue (Alldredge et al., 1993; Engel, 2009; Passow, 2002). TEP enhances particle aggregation due to their stickiness (Iversen, 2023; Wurl and Cunliffe, 2017), resulting in the carbon transfer from the DOC to the POC pool (Alldredge and Crocker, 1995; Passow, 2002), and as such, TEP are regarded as essential components of the organic carbon cycle in the ocean (Verdugo, 2021). Moreover, TEP and other organic particles can be transported into the atmosphere, where they serve as precursors to biogenic aerosols that influence cloud formation and microphysical processes (Irish et al., 2017; Lawler et al., 2021; Leck and Bigg, 2005; Orellana et al., 2011; Porter et al., 2022; van Pinxteren et al., 2022; Wilson et al., 2015). In remote marine regions, particularly the Arctic, organic compounds emitted from the upper ocean can serve as an important source of particles, thereby influencing the cloud feedback mechanisms and the overall radiation budget (Hamacher-Barth et al., 2016; Goosse et al., 2018; Hartmann et al., 2020; Ickes et al., 2020).

The remote and harsh conditions of the Arctic Ocean severely limit the feasibility of *in situ* measurements, making it challenging to understand and monitor the precise dynamics of TEP formation, distribution and variability (Engel et al., 2020; Zamanillo et al., 2019). Numerical models are essential tools for qualitatively and quantitatively understanding organic carbon dynamics, filling the gap left by observations. Thus, accurate, high-resolution numerical models are needed to predict TEP dynamics, elucidate their role in the Arctic organic carbon cycle, and evaluate their potential feedback mechanisms within the Earth system. However, modeling TEP is particularly challenging due to the complex interplay of factors that govern their production, transport, and decomposition (Wurl et al., 2011), but also of their nature as a marine gel (Engel et al., 2020; Verdugo, 2021).

To our knowledge, the formation, aggregation, and remineralization of PCHO and TEP as organic carbon pools in the upper ocean have not yet been explicitly integrated into global ocean biogeochemistry models or Earth System Models. In particular, current Earth System Models mostly neglect the possible feedback effects of marine organic emissions (Taylor et al., 2022). Furthermore, primary marine organic aerosol is not specifically treated in most aerosol–climate models and often only presented as POC. Alternatively, parameterizations merely relate marine organic aerosol emission to total Chlorophyll *a*

https://doi.org/10.5194/egusphere-2025-4190
Preprint. Discussion started: 4 October 2025

(TChla) in the surface ocean waters (Zhao et al., 2021), which is a clear oversimplification ignoring bacteria-induced or stress-related productions. Therefore, including marine biogenic particles in Earth System Models is expected to improve cloud representation (Schmale et al., 2021). The first steps to parameterizing the ocean–atmosphere transport of marine organic particles have been proposed by the OCEANFILMS (Organic Compounds from Ecosystems to Aerosols: Natural Films and Interfaces via Langmuir Molecular Surfactants) parameterization by Burrows et al. (2014) and further developed by Leon-Marcos et al. (2025).

With an emphasis on the Arctic Ocean, the present study assesses the implementation of PCHO and TEP in a state-of-the-art global ocean biogeochemistry model, the third version of the Regulated Ecosystem Model (REcoM3; Gürses et al., 2023; Oziel et al., 2025) coupled to the Finite volumE sea-ice ocean circulation model FESOM2.1 (Danilov et al., 2017). REcoM3 is a flexible stoichiometry model (i.e. it does not use fixed Redfield stoichiometry) enabling it to represent carbon overconsumption under nutrient-depleted conditions as one major pathway for the formation of PCHO. The scheme is based on the TEP aggregation model developed by Engel et al. (2004) and first results of the current setup have been presented in Leon-Marcos et al. (2025). In contrast to other ocean biogeochemistry models, the FESOM2.1–REcoM3 configuration offers the advantage of an unstructured grid, which allows for higher resolution in the Arctic while also simulating the entire global ocean. This approach goes beyond several other modeling studies that have parametrized POC size distributions instead of TEP formation mainly when investigating particle export to the deep ocean, e.g., by implementing a power-law distribution of particle sizes, or several size classes of POC with different sinking parameterization (Kriest and Evans, 1999; Gehlen et al., 2006; Maerz et al., 2020). Another approach proposed 20 different aggregate classes, which can be applicable in a single-column model (Jokulsdottir and Archer, 2016), but would not be feasible for a large-scale ocean biogeochemistry model.

Our study evaluates the implementation of PCHO and TEP into FESOM2.1–REcoM3 by assessing the model performance in simulating the seasonal dynamics in the upper Arctic Ocean in comparison to observational datasets. Since in the model parameterization, PCHO, the precursor of TEP, is produced during primary production, we first assess the performance of this parametrization by investigating the phytoplankton Chlorophyll *a* distribution in the entire Arctic Ocean and examining the bloom phenology in the Fram Strait, as an example of a region rich in in situ measurements. We subsequently assess the occurrence patterns of PCHO and TEP throughout the Arctic Ocean using observational datasets available to us. Lastly, we contextualize the simulation results within the broader context of the global ocean.

2 Methods

2.1 Model setup

The coupling of FESOM2.1–REcoM3 is a state-of-the-art ocean biogeochemistry model. It performs reasonably well both on a global scale (Friedlingstein et al., 2023; Gürses et al., 2023; Hauck et al., 2020; Karakuş et al., 2021, 2022; Schourup-Kristensen et al., 2014) and in various regional applications (Hauck et al., 2013; Nissen et al., 2022, 2023, 2024; Oziel et al., 2022; Schourup-Kristensen et al., 2018, 2021). The ocean biogeochemistry model REcoM3 has also recently been included

https://doi.org/10.5194/egusphere-2025-4190
Preprint. Discussion started: 4 October 2025

into the AWI Climate Model (Semmler et al., 2020; Streffing et al., 2022), an Earth System Model, to which computational performance is critical.

This study builds upon the FESOM2.1–REcoM3 setup of Oziel et al. (2025) which is optimized in its parameterizations for the Arctic Ocean, for which the Arctic biogeochemistry has previously been successfully simulated with regard to primary production, light and nutrient availability (Oziel et al., 2022; Schourup-Kristensen et al., 2018, 2021). The current setup includes parameterizations for aeolian and riverine nitrogen input, and benthic denitrification (Schourup-Kristensen et al., 2018). The photo-damage parameterization (Álvarez et al., 2019) is turned off, which was developed for a global setup that was found to lead to a TChla concentration that was too high in the Arctic (Oziel et al., 2025). This study contains the following changes compared to Oziel et al. (2025), which have already been presented in Leon-Marcos et al. (2025):

- The cycle of organic carbon is specified in greater detail through the dissolved, particulate and intracellular carbon pools by adding the process description for PCHO and TEP, following Engel et al. (2004) and Schartau et al. (2007) as presented in Sect. 2.2. The model now includes 30 different biogeochemical tracers.
- The aggregation of phytoplankton to detritus is made dependent of TEP concentration, as an attempt to represent the effect of TEP on particle stickiness.

This simulation is based on the *fARC* mesh, an irregular grid, resolving the Arctic region with a resolution of approximately 4.5 km (north of 60° N), and stepwise decreasing resolution (20-120 km) from the coasts and productive areas to the subtropical gyres (Oziel et al., 2022, 2025; Schourup-Kristensen et al., 2018; Wang et al., 2016, 2018; Wekerle et al., 2017). Simulations are carried out for the period 1958 to 2019, i.e., a total of 61 years, with atmospheric forcing from the atmospheric reanalysis datasets of JRA55-do v.1.4.0 (Tsujino et al., 2018). The ocean simulation is initialized from temperature and salinity fields of the Polar Science Center Hydrographic Climatology (Steele et al., 2001), the biogeochemical simulation from initial fields of dissolved inorganic nitrogen (DIN) and dissolved silicic acid concentration of the World Ocean Atlas climatology (Garcia et al., 2019a, b), and dissolved inorganic carbon (DIC) and alkalinity of the Global Ocean Data Analysis Project version 2 (Lauvset et al., 2016). Riverine inputs of inorganic and organic carbon and nitrogen are derived from Terhaar et al. (2021).

The period 1958 to 1990 is considered as spin-up, which allows the biological processes in the surface ocean to reach quasi-equilibrium and with it the concentration of labile organic carbon compounds; thus, the period of 1990 to 2019 is analyzed. Monthly output is obtained for all years, and daily output for April to September 2017 for comparison to in situ observations of May to July 2017 from the ship-based *Physical feedbacks of Arctic Boundary Layer Sea ice, Cloud And Aerosol (PASCAL)* campaign PS106 on RV *Polarstern*. A campaign overview is presented in Macke and Flores (2018) and Wendisch et al. (2019).

2.2 Implementation of PCHO and TEP

This section details the approach of PCHO and TEP implementation into the cycle of organic carbon through the ecosystem as simulated in REcoM3, while quickly recapitulating the relevant state equations and processes. The reader is referred to the overview publication on REcoM3 by Gürses et al. (2023) for an extensive description of all the biogeochemical model processes.

https://doi.org/10.5194/egusphere-2025-4190
Preprint. Discussion started: 4 October 2025

Engel et al. (2004) and Schartau et al. (2007) developed generalized equations and a parameterization for phytoplankton carbon exudation and for aggregation of organic carbon particles. A quantitative description of these processes and related parameters was obtained by fitting a zero-dimensional version of REcoM (Schartau et al., 2007) to data from a mesocosm experiment (Engel et al., 2004). Further, Schartau et al. (2007) conducted a parameter optimization for REcoM. The PCHO and TEP pools were omitted in recent model releases on the global scale but re-integrated as part of this study.

In a first step, organic carbon is built up by photosynthesis in small phytoplankton and diatoms and exuded in the form of two different dissolved, labile pools: PCHO and residual DOC (considered as consisting of labile organic compounds, but the chemical composition is not specified in greater detail). In a second step, multiple PCHO molecules may form aggregates or react with already existing TEP. Both DOC and TEP are remineralized to DIC. These processes are detailed out further below with respect to the simulated state equations. Following the organic carbon further, a part of the phytoplankton carbon is lost to detritus via aggregation and grazing by the zooplankton. Additionally, the two simulated zooplankton classes contribute to the build-up of detritus through sloppy feeding and mortality, but graze on these detritus particles as well. A surplus of organic carbon is excreted by zooplankton to DOC. Detritus particles can either be degraded to DOC or sink down into the water column, finally reaching the benthic layer.

The state equation for phytoplankton carbon (shown here for small phytoplankton, C_{phy}, as an example case) is given in Eq. 1 following the REcoM3 introduction by Gürses et al. (2023). It states that net photosynthesis contributes to the increase of C_{phy}, whereas aggregation of phytoplankton leads to formation of detritus (c.f. Eq. 5). Exudation of organic carbon and grazing by zooplankton reduces C_{phy}:

$$S(C_{phy}) = \underbrace{(P_{phy} - r_{phy}) \cdot C_{phy}}_{\text{net photosynthesis}} \underbrace{- g \cdot C_{phy}}_{\text{aggregation}} \underbrace{- \varepsilon^{C}_{phy} \cdot f^{lim}_{phy} \cdot C_{phy}}_{\text{exudation}} \underbrace{- G^{zoo1}_{phy} - G^{zoo2}_{phy}}_{\text{grazing by small \& macrozoo.}} , \tag{1}$$

where the limitation terms and aggregation processes used in this state equation are presented below (Eq. 5–7). An explanatory list of state variables and parameters mentioned in this section can be found in Tab. 1 and 2. Tab. 3 contains the terms leading to local sources and sinks of the biogeochemical state variables as presented in Gürses et al. (2023).

The DOC sources are represented by the release of organic carbon by two phytoplankton classes and two zooplankton classes, and degradation of organic carbon from both detritus classes. The remineralization to DIC is the only sink for DOC. The simulated source-minus-sink term is given as

$$S(C_{DOC}) = \underbrace{(1 - f_{PCHO}) \cdot \varepsilon^{C}_{phy} \cdot f^{lim}_{phy} \cdot C_{phy}}_{\text{exudation by small phytoplankton}} \underbrace{+ (1 - f_{PCHO}) \cdot \varepsilon^{C}_{dia} \cdot f^{lim}_{dia} \cdot C_{dia}}_{\text{exudation by diatoms}} \underbrace{+ \varepsilon^{C}_{zoo1} \cdot C_{zoo1}}_{\text{excretion by small zoo.}} \underbrace{+ \varepsilon^{C}_{zoo2} \cdot C_{zoo2}}_{\text{excretion by macrozoo.}} \tag{2}$$
$$\underbrace{+ \rho_{DetC} \cdot f_T \cdot C_{det1} + \rho_{DetC} \cdot f_T \cdot C_{det2}}_{\text{detritus degradation}} \underbrace{- \rho_{DOC} \cdot f_T \cdot C_{DOC}}_{\text{remineralization to DIC}} .$$

https://doi.org/10.5194/egusphere-2025-4190
Preprint. Discussion started: 4 October 2025

We implemented carbon-based source-minus-sink terms for PCHO and TEP into the current REcoM version 3 based on Engel et al. (2004) and Schartau et al. (2007) with

$$S(C_{PCHO}) = \underbrace{f_{PCHO} \cdot \varepsilon^{C}_{phy} \cdot f^{lim}_{phy} \cdot C_{phy}}_{\text{exudation by small phytoplankton}} + \underbrace{f_{PCHO} \cdot \varepsilon^{C}_{dia} \cdot f^{lim}_{dia} \cdot C_{dia}}_{\text{exudation by diatoms}} \tag{3}$$

$$\underbrace{-\alpha_{PCHO} \cdot \beta_{PCHO} \cdot C_{PCHO} \cdot C_{PCHO}}_{\text{aggregation of PCHO with PCHO}} \underbrace{-\alpha_{TEP} \cdot \beta_{TEP} \cdot C_{PCHO} \cdot C_{TEP}}_{\text{aggregation of PCHO with TEP}},$$

$$S(C_{TEP}) = \underbrace{\alpha_{PCHO} \cdot \beta_{PCHO} \cdot C_{PCHO} \cdot C_{PCHO}}_{\text{aggregation of PCHO with PCHO}} + \underbrace{\alpha_{TEP} \cdot \beta_{TEP} \cdot C_{PCHO} \cdot C_{TEP}}_{\text{aggregation of PCHO with TEP}} \tag{4}$$

$$\underbrace{-\rho_{TEP} \cdot f_T \cdot C_{TEP}}_{\text{remineralization to DIC}}.$$

A fraction of the exuded organic carbon by small phytoplankton and diatoms builds up the PCHO pool, while the aggregation of PCHO with other PCHO molecules or with already existing TEP removes PCHO (Eq. 3). These aggregation processes are described via a two-size class model for PCHO and TEP. The equations were derived from the Smoluchowski equations for the cluster-to-cluster aggregation of the individual polymer molecules by summation of the carbon content in the different molecule size classes contributing to the PCHO and TEP pool, respectively. Mathematically, this is done by introducing a Heaviside step function which defines the size class for the distinction of PCHO and TEP (Engel et al., 2004; Von Smoluchowski, 1917; Ziff and Stell, 1980). The resulting equations depend on the concentrations of PCHO and TEP, on the stickiness of the substrates, and on the carbon specific collision kernels for PCHO–PCHO and PCHO–TEP interaction (Eq. 4, c.f. Engel et al., 2004). The carbon-specific collision kernels describe the probability of encounter of molecules via molecular diffusion. In this approach, the values of these kernels are parametrized as the collision rate parameters β_{PCHO} and β_{TEP} (Engel et al., 2004). Consequently, the TEP pool is increased by aggregation products of PCHO–PCHO and PCHO–TEP. So far, only the bacterial remineralization to DIC (described for simplicity as a temperature-dependent linear loss rate) is considered as sink for TEP (Eq. 4).

The limiter functions f^{lim}_{phy} and f^{lim}_{dia} are given exemplarily for small phytoplankton as

$$f^{lim}_{phy} = 1 - exp(-\theta^{N}_{max} \cdot (\mid \Delta q \mid - \Delta q)^2), \tag{5}$$

$$\Delta q = q^{N:C_{max}}_{phy} - q^{N:C}_{phy} \tag{6}$$

and regulate the phytoplankton metabolic processes via a non-linear function based on the intracellular nitrogen to carbon ratio (N:C ratio) following Geider et al. (1998) and modified for REcoM (Sect. A6.1 in Schourup-Kristensen et al., 2014). The functions for diatoms have a similar structure; parameter values are given in Tab. 4. The limiter function is zero for N:C ratios above the value of N:C $= 21.2 : 106 = 0.2$. No nitrogen uptake and no carbon exudation take place in this case. When the N:C ratio becomes lower, the limiter function increases, hence both nitrogen uptake and carbon exudation of phytoplankton begin. When the current N:C ratio is lower than the Redfield ratio (N:C $= 16 : 106 = 0.151$), the limiter function is one, not limiting uptake nor exudation.

https://doi.org/10.5194/egusphere-2025-4190
Preprint. Discussion started: 4 October 2025

Table 1. State variables used in the model implementation of small phytoplankton carbon (C_{phy}), dissolved organic carbon (DOC), dissolved acidic polysaccharides (PCHO), and transparent exopolymer particles (TEP).

State variable	Description	Unit
C_{phy}	carbon concentration of small phytoplankton	$\mathrm{mmol\,C\,m^{-3}}$
C_{dia}	carbon concentration of diatoms	$\mathrm{mmol\,C\,m^{-3}}$
C_{zoo1}	carbon concentration of small zooplankton	$\mathrm{mmol\,C\,m^{-3}}$
C_{zoo2}	carbon concentration of polar macrozooplankton	$\mathrm{mmol\,C\,m^{-3}}$
C_{det1}	carbon concentration of detritus class 1	$\mathrm{mmol\,C\,m^{-3}}$
C_{det2}	carbon concentration of detritus class 2	$\mathrm{mmol\,C\,m^{-3}}$
C_{DOC}	carbon concentration of DOC	$\mathrm{mmol\,C\,m^{-3}}$
C_{PCHO}	carbon concentration of PCHO	$\mathrm{mmol\,C\,m^{-3}}$
C_{TEP}	carbon concentration of TEP	$\mathrm{mmol\,C\,m^{-3}}$
N_{phy}	nitrogen concentration of small phytoplankton	$\mathrm{mmol\,N\,m^{-3}}$
N_{dia}	nitrogen concentration of diatoms	$\mathrm{mmol\,N\,m^{-3}}$
N_{det1}	nitrogen concentration of detritus class 1	$\mathrm{mmol\,N\,m^{-3}}$
N_{det2}	nitrogen concentration of detritus class 2	$\mathrm{mmol\,N\,m^{-3}}$

The aggregation rate determines the amount of small phytoplankton and diatom carbon transferred to the detritus pool in the phytoplankton state equation (Eq. 1). The aggregation rate g in Eq. 7 was calculated based on REcoM3 (Eq. A42 in Gürses et al., 2023) with a new term describing the particle stickiness depending on TEP concentration (Eq. B13 in Schartau et al., 2007). The aggregation loss for phytoplankton and detritus classes is based on their corresponding nitrogen concentration. Additionally, the aggregation loss for diatoms depends on nutrient limitation mimicking diatom mucus production (Aumont et al., 2015; Gürses et al., 2023; Waite et al., 1992). High TEP concentrations (C_{TEP}) increase the particle stickiness based on a Michaelis-Menten-type term and, thus, increase the aggregation rate g:

$$g = (\phi_{PP} \cdot (N_{phy} + (1 - q_{dia}^{lim}) \cdot N_{dia}) + \phi_{PD} \cdot (N_{det1} + N_{det2})) \cdot \frac{C_{TEP}}{k_{TEP} + C_{TEP}} \tag{7}$$

2.3 Processing of simulation results

Analysis is carried out for the Arctic Ocean and contextualized within a global perspective. Boundaries for the Arctic Ocean basins and seas (Fig. 1) are set according to Nöthig et al. (2020) and Randelhoff et al. (2020).

The upper 30 m of the ocean are considered for volume-weighted mean concentration of model variables, a depth range which roughly corresponds to the summer mixed layer depth in the Arctic Ocean (Peralta-Ferriz and Woodgate, 2015) following the definition of Monterey and Levitus (1997). The surface microlayer, where organic particles are expected to get enriched in a natural ecosystem, is neglected in the current model setup. The volume-weighted mean concentration $\overline{c}_{vw}$ for each grid cell

https://doi.org/10.5194/egusphere-2025-4190
Preprint. Discussion started: 4 October 2025

Table 2. Parameters used in the model implementation of small phytoplankton carbon (C_{phy}), dissolved organic carbon (DOC), dissolved acidic polysaccharides (PCHO), and transparent exopolymer particles (TEP).

Parameter	Description	Value	Unit
α_{PCHO}	stickiness for PCHO-PCHO	0.00087	[]
α_{TEP}	stickiness for PCHO-TEP	0.4	[]
β_{PCHO}	C-based collision rate parameter for PCHO-PCHO	0.86	$\mathrm{m^3\,mmol\,C^{-1}\,d^{-1}}$
β_{TEP}	C-based collision rate parameter for PCHO-TEP	0.064	$\mathrm{m^3\,mmol\,C^{-1}\,d^{-1}}$
ε^C_{phy}	exudation rate constant for small phytoplankton	0.1	$\mathrm{d^{-1}}$
ε^C_{dia}	exudation rate constant for diatoms	0.1	$\mathrm{d^{-1}}$
ε^C_{zoo1}	excretion rate constant for small zooplankton	0.15	$\mathrm{d^{-1}}$
ε^C_{zoo2}	excretion rate constant for polar macrozooplankton	0.02	$\mathrm{d^{-1}}$
ρ_{DetC}	degradation rate constant for detritus	0.15	$\mathrm{d^{-1}}$
ρ_{DOC}	remineralization rate constant for DOC	0.1	$\mathrm{d^{-1}}$
ρ_{TEP}	remineralization rate constant for TEP	0.1	$\mathrm{d^{-1}}$
ϕ_{PP}	N-based max. aggregation loss parameter for plankton	0.015	$\mathrm{m^3\,mmol\,N^{-1}\,d^{-1}}$
ϕ_{PD}	N-based max. aggregation loss parameter for detritus	0.165	$\mathrm{m^3\,mmol\,N^{-1}\,d^{-1}}$
θ^N_{max}	max. limiter regulator for N	1000	$\mathrm{mmol\,C\,mmol\,N^{-1}}$
f_{PCHO}	fraction of PCHO of exuded organic carbon	0.634	[]
k_{TEP}	half-saturation const. of TEP controlled particle stickiness for aggregation of phytoplankton cells	45.0	$\mathrm{mmol\,C\,m^{-3}}$
$q^{N:C_{max}}_{phy}$	max. intracellular N:C ratio for small phytoplankton	0.2	$\mathrm{mmol\,N\,mmol\,C^{-1}}$

is calculated as

$$\bar{c}_{vw} = \frac{\sum_i A \cdot d_i \cdot c_i}{V_{tot}} \tag{8}$$

over the depth range depending on the total volume V_{tot}

$$V_{tot} = \sum_i A_i \cdot d_i \tag{9}$$

with area A_i and thickness d_i of layer with index i, and concentration c_i corresponding to that layer.

An overall spatial mean and the 0.25, 0.5, and 0.75 quantile concentrations are computed using these monthly volume-weighted mean data. A standard deviation and coefficient of variation are calculated from the volume-weighted mean over the monthly time steps. Differing from this depth range, volume-weighted mean concentrations of simulated TEP are calculated over the same depth range as stated for observational datasets when comparing to these. The standard deviation is calculated over the grid points inside the area of concern and over the specific month corresponding to the observation data used. Volume-weighted mean TEP concentrations of the time frame 1990 to 2019 are provided as binned product according to Longhurst provinces (Longhurst, 2006) in Supplementary Tab. A2 to enable a comparison to upcoming studies.

https://doi.org/10.5194/egusphere-2025-4190
Preprint. Discussion started: 4 October 2025

Table 3. Model variables used in Eq. 1 (C_{phy}), Eq. 2 (C_{DOC}), and Eq. 7 (g) following Gürses et al. (2023). The equation numbers in the last column refer to the equation numbers in Gürses et al. (2023). The corresponding parameters are listed in Tab. 4.

		Model variable	Description	Eq.
P_{phy}	=	$P_{phy}^{max} \cdot \left(1 - exp\left(\frac{-\alpha_{phy} \cdot q^{Chl:C} \cdot PAR}{P_{phy}^{max}}\right)\right)$	photosynthesis rate for small phytoplankton	A36
r_{phy}	=	$res_{phy} \cdot f_{phy}^{lim} + \zeta \cdot V_{phy}^{N}$	respiration rate (respiration + biosynthesis costs) for small phytoplankton	A38
G_{phy}^{zoo1}	=	$q_{phy}^{C:N} \cdot G_{tot}^{zoo1} \cdot \frac{\rho_{phy} \cdot N_{phy}}{\sum_i \cdot N_i}$	grazing rate of small zooplankton on small phytoplankton	A54
G_{phy}^{zoo2}	=	$q_{phy}^{C:N} \cdot G_{tot}^{zoo2} \cdot \frac{\rho_{phy} \cdot N_{phy}}{\sum_i \cdot N_i}$	grazing rate of macrozooplankton on small phytoplankton	A54
f_T	=	$exp\left(-4500 \cdot \left(\frac{1}{T} - \frac{1}{T_{ref}}\right)\right)$	temperature-dependent Arrhenius function	A33
q_{dia}^{lim}	=	$min(f_{lim,dia}^{Fe}, f_{lim,dia}^{N:C_{min}}, f_{lim,dia}^{Si:C_{min}})$	nutrient limitation factor for diatoms	A43

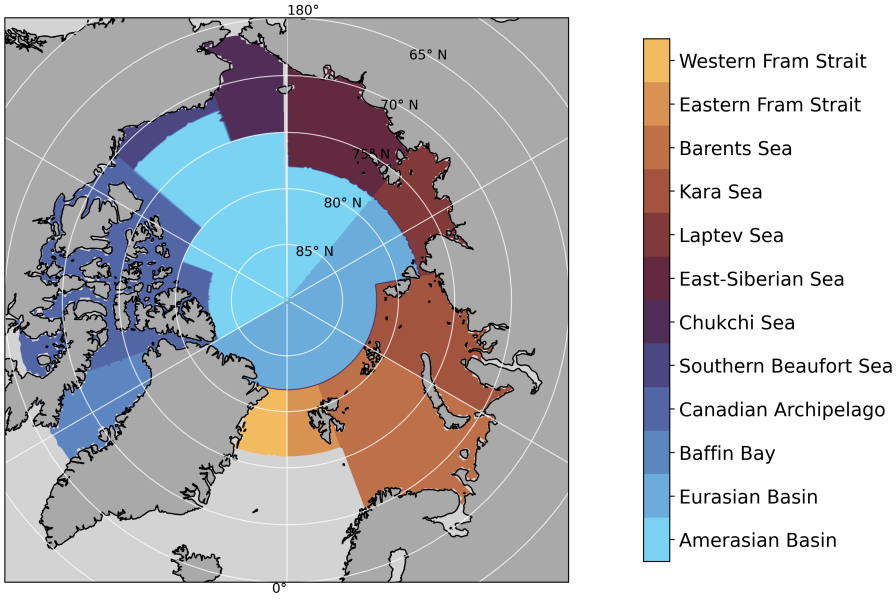

Figure 1. Map of Arctic Ocean basins and seas for evaluation of biogeochemical properties in this study. The regional boundaries are constructed based on Nöthig et al. (2020) and Randelhoff et al. (2020).

https://doi.org/10.5194/egusphere-2025-4190
Preprint. Discussion started: 4 October 2025

Table 4. List of variables and parameters used in description of model processes within the description of terms presented in Tab. 3. The equation numbers in brackets refer to the equation numbers in Gürses et al. (2023).

Model variable	Description		Unit
$f_{lim,dia}^{Fe}$	iron limiter function for diatoms (A48)		
$f_{lim,dia}^{N:C_{min}}$	nitrogen limiter function for diatoms (A49)		
$f_{lim,dia}^{Si:C_{min}}$	silicate limiter function for diatoms (A46)		
G_{tot}^{zoo1}	total zooplankton grazing rate		$\mathrm{mmol\,N\,m^{-3}\,d^{-1}}$
G_{tot}^{zoo2}	total macrozooplankton grazing rate		$\mathrm{mmol\,N\,m^{-3}\,d^{-1}}$
N_i	nitrogen concentration of variable *i*		$\mathrm{mmol\,N\,m^{-3}}$
PAR	photosynthetically available radiation		$\mathrm{W\,m^{-2}}$
P_{phy}^{max}	C-specific light-saturated rate of photosynthesis		$\mathrm{d^{-1}}$
$q^{Chl:C}$	current intracellular ratio of Chlorophyll *a* to carbon		$\mathrm{mg\,Chl\,mmol\,C^{-1}}$
$q_{phy}^{C:N}$	current intracellular C:N ratio		$\mathrm{mmol\,N\,mmol\,C^{-1}}$
T	local temperature		K
V_{phy}^{N}	N-assimilation rate of small phytoplankton		$\mathrm{mmol\,N\,m^{-3}\,d^{-1}}$
Parameter	**Description**	**Value**	**Unit**
α_{phy}	light-harvesting efficiency for small phyto.	0.14	$\mathrm{mmol\,C\,m^2\,(mg\,Chl\,W\,d)^{-1}}$
ζ	cost of biosynthesis of N	2.33	$\mathrm{mmol\,C\,mmol\,N^{-1}}$
ρ_{phy}^{zoo1}	grazing preference of zoo. for small phyto.	1.0	[]
ρ_{phy}^{zoo1}	grazing preference of macrozoo. for small phyto.	0.5	[]
res_{phy}	maintenance respiration rate constant for small phytoplankton	0.01	$\mathrm{d^{-1}}$
T_{ref}	reference temperature for Arrhenius function	288.15	K

2.4 Remote-sensing products for model evaluation

To evaluate the performance of the simulation, the model is compared to various in situ or remote-sensing datasets, which are obtained directly from the cited literature and repositories. The Copernicus Marine Environment Monitoring Service level 4 monthly reprocessed Arctic Ocean Color product (Product ID: OCEANCOLOUR_ARC_BGC_L4_MY_009_124) — CMEMS, in the following— provides estimates for TChla in the upper ocean with a resolution of 1 km (Copernicus Marine Service, 2022) and is available at the Copernicus Marine Data Store at https://data.marine.copernicus.eu/product/OCEANCOLOUR_ARC_BGC_L4_MY_009_124/. The CMEMS TChla error is provided by Copernicus and is defined as the standard deviation derived from daily TChla datapoints of the corresponding month. Matching the last two decades of the simulation, monthly CMEMS data of 2000 to 2019 is downloaded and processed by averaging to a summer (May to September) mean concentration for TChla and its standard deviation. Both CMEMS and FESOM2.1–REcoM3 data are interpolated to a regular grid of 0.2 degrees for comparison. Likewise, the Arctic Ocean TChla product based on the algorithm *AOreg.emp*

https://doi.org/10.5194/egusphere-2025-4190
Preprint. Discussion started: 4 October 2025

from Lewis and Arrigo (2020) is retrieved as a supplementary comparison for TChla, composed of the years 2003 to 2019, of which the Modis/Aqua TChla only is processed.

2.5 In situ datasets for model evaluation

Since satellite TChla products have quite large uncertainties of 25 to 150 % (Seegers et al., 2018; Xi et al., 2021) and standard deviations (Fig. 2 panel d on CMEMS and Supplementary Fig. A1 panel d on Lewis and Arrigo, 2020) in the Arctic Ocean, we also compare the FESOM2.1–REcoM3 simulation to in situ observations. A valuable dataset for the model evaluation is the long-term compilation of in situ observation data of TChla in the Fram Strait and adjacent Arctic seas covering mainly the summer months May to September 1991 to 2015, presented in Nöthig et al. (2020). Following this study, the results of the simulation are split into box plots for different Arctic regions, summarizing the summer months May to September of 2000 to 2019 (to match the time frame of remote-sensing comparison consistently) and evaluated for the upper 100 m depth-integrated data.

The simulated PCHO represents the acidic dissolved combined carbohydrates, which are reported to form a major part of dissolved carbohydrates in the ocean (Gao et al., 2012; Krembs and Deming, 2008), and are complemented by a small fraction of dissolved free carbohydrates (various monosaccharides). Since explicit in situ measurements of PCHO are not available, simulated PCHO concentrations were compared to in situ observations of dissolved combined carbohydrates (DCCHO). DCCHO are typically measured as individual monosaccharides released from oligo- and polysaccharides, including PCHO, after acid hydrolysis. A small DCCHO mass contribution originates from monosaccharides with acidic moieties, such as carboxyl groups in uronic acids (e.g., von Jackowski et al., 2020; Zeppenfeld et al., 2021, 2023b). However, PCHO may also contain acidity from sulfate and phosphate side groups, which are not detected using the DCCHO chromatographic protocol after acid hydrolysis with hydrochloric acid (Zeppenfeld et al., 2020; Engel and Händel, 2011). The exact combination of monosaccharide units within a combined carbohydrate often remains unclear (Arnosti et al., 2021). Therefore, it can be assumed that a significantly higher proportion of DCCHO could be attributed to PCHO than is directly apparent from the measurements. As such, a comparison of PCHO and DCCHO appears valid. PCHO and DCCHO concentrations are expected to be within the same order of magnitude.

The dataset of in situ DCCHO presented here is published as Zeppenfeld et al. (2023a) and available at https://doi.pangaea.de/10.1594/PANGAEA.961004. It is derived from field bulk water samples collected at one meter depth during the PASCAL campaign on RV *Polarstern* following the protocol of Zeppenfeld et al. (2020) in 2017, using high-performance anion exchange chromatography coupled with pulsed amperometric detection (HPAEC-PAD). For the validation, the in situ DCCHO concentrations are differentiated into three groups: (a) ice-free ocean, (b) marginal ice zone (MIZ), and (c) leads/polynyas within the ice pack. For the model validation, only the mean and standard deviations of DCCHO concentrations from each of the three groups are considered.

TEP can be determined in water samples observationally by microscopy of the abundances of particles [$\#\,\mathrm{L}^{-1}$], by the determination of particle surface area [$\mathrm{cm}^2\,\mathrm{L}^{-1}$] (Engel, 2009; Engel et al., 2020), or colorimetrically by staining with Alcian Blue solution resulting in Xanthan gum equivalents [$\mu\mathrm{g\,Xeq\,L}^{-1}$] (Alldredge et al., 1993; Engel, 2009). As these methods are

https://doi.org/10.5194/egusphere-2025-4190
Preprint. Discussion started: 4 October 2025

not fully comparable to one another—even considered unreliable (Discart et al., 2015)—colorimetrically determined in situ TEP is prioritized in this study, as variations in TEP measurement methods can lead to inconsistent comparability (Discart et al., 2015). Data on in situ TEP concentration are converted to [$\mu g\,C\,L^{-1}$], as explained below, as REcoM3 biogeochemical processes are described in units of carbon. Namely, the datasets of Engel et al. (2020), Olli et al. (2007), von Jackowski et al. (2020), Wurl et al. (2011), and Yamada et al. (2015) are used. Furthermore, the TEP concentration given in Yamada et al. (2015) is converted from Xanthan gum equivalents [$\mu g\,Xeq\,L^{-1}$] to carbon [$\mu g\,C\,L^{-1}$] by a factor of $f_{conv} = 0.05 \frac{mol\,C}{g\,Xeq} \cdot 12.01 \frac{g}{mol}$ following the review of Engel et al. (2020).

3 Results

Within this study, we assess the formation and degradation processes of PCHO and TEP in FESOM2.1–REcoM3 (Gürses et al., 2023). While Gürses et al. (2023) present a global model setup, the specific setup in this study is optimized in its parameterizations for the Arctic Ocean, for which the Arctic biogeochemistry has previously been successfully simulated with regard to primary production, light and nutrient availability (Oziel et al., 2022; Schourup-Kristensen et al., 2018, 2021). In the following sections, we present key biogeochemistry quantities in the Arctic Ocean based on our new simulation with a two-size class parametrization of TEP formation. The particular focus of model assessment is put on phytoplankton distribution in terms of TChla and POC concentrations (Sect. 3.1) and the link of phytoplankton phenology to the simulated PCHO (Sect. 3.2). Section 3.3 focuses on TEP concentration results. Finally, we present the perspectives of the newly developed FESOM2.1–REcoM3 setup for global applications in Sect. 3.4.

3.1 Total Chlorophyll *a* and Particulate Organic Carbon

The Arctic setup of FESOM2.1–REcoM3 simulates the phytoplankton seasonal cycle, where phytoplankton depends on nutrient and light availability and is controlled by zooplankton grazing, aggregation, and degradation losses. This is later discussed in comparison with remote-sensing products and in situ observations of the Arctic Ocean.

Figure 2 displays the phytoplankton biomass in the surface Arctic Ocean in terms of TChla from the FESOM2.1–REcoM3 simulation and compares it to the CMEMS Arctic satellite re-analysis product. The data is averaged over the years 2000 to 2019 (as a mean model state) for the months May to September when satellite data are available. FESOM2.1–REcoM3 simulates highest TChla concentrations of up to $6\,mg\,m^{-3}$ along the Siberian coast and in other shelf seas between 0.5 and $3\,mg\,m^{-3}$ (Fig. 2 panel a). In the Fram Strait, TChla range from 1 to $3\,mg\,m^{-3}$ with highest concentration in its central part, while in the central basins of the Arctic Ocean, TChla is generally low, with concentrations of up to $0.8\,mg\,m^{-3}$.

The CMEMS TChla product shows no coverage of the central Arctic Ocean due to the satellite sensors configuration not enabling observations at these high latitudes (Fig. 2 panel b). In the Barents, Kara, and Laptev Seas, TChla ranges from 0.5 to $5\,mg\,m^{-3}$, with peaks of up to $15\,mg\,m^{-3}$ close to the coastline. In the East Siberian, Chukchi, and Beaufort Seas, the concentration of TChla is lower, ranging from 0.1 to $1\,mg\,m^{-3}$, also with very high concentration close to the coast. The

https://doi.org/10.5194/egusphere-2025-4190
Preprint. Discussion started: 4 October 2025

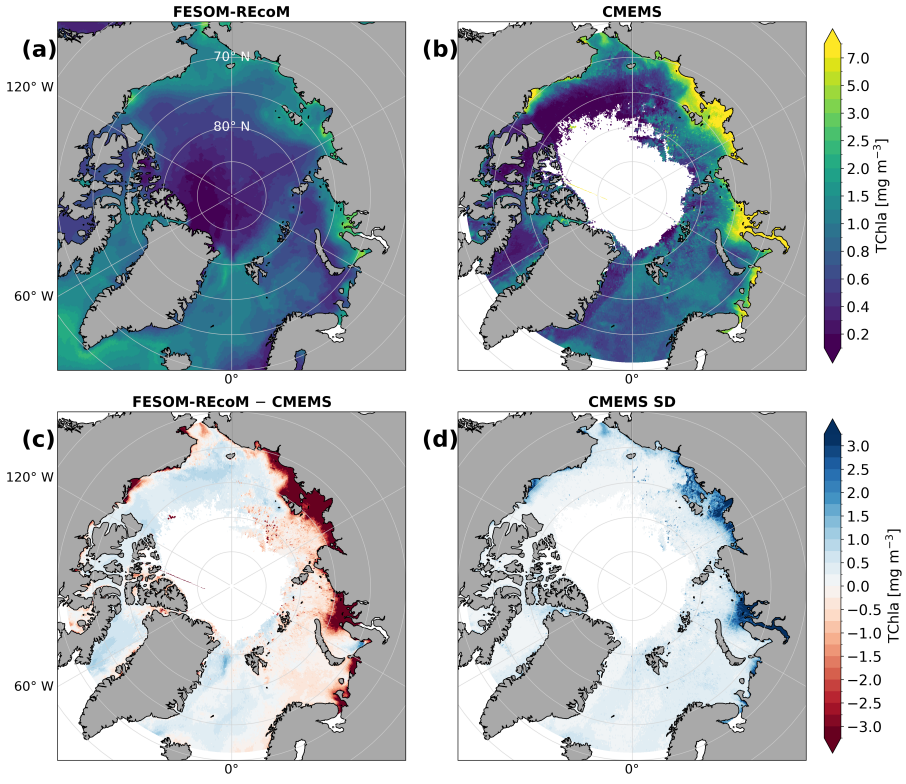

Figure 2. Maps of surface total Chlorophyll *a* (TChla) of FESOM2.1–REcoM3 (panel a), of the CMEMS Arctic re-analysis product (panel b), the difference of CMEMS to the model results (panel c), and the standard deviation of CMEMS (panel d) as average of May to September of the years 2000 to 2019. CMEMS data does not cover the central Arctic Ocean.

standard deviation of TChla from the CMEMS TChla product is mostly lower than $0.5\,\mathrm{mg\,m^{-3}}$. However, it increases to more than $2\,\mathrm{mg\,m^{-3}}$ along the coastline (Fig. 2 panel d).

Compiling the TChla concentrations as in Nöthig et al. (2020), they range from close to zero to $69.2\,\mathrm{mg\,m^{-2}}$ regarding first to third quartile, with the highest median of $40.4\,\mathrm{mg\,m^{-2}}$ in the eastern Fram Strait. In the western Fram Strait and in the Siberian seas, TChla median concentration ranges from 24.5 to $32.9\,\mathrm{mg\,m^{-2}}$. In the Eurasian and Amerasian Basins, median concentration is close to $0\,\mathrm{mg\,m^{-2}}$ with first to third quartile spanning the range 0.002–$14.2\,\mathrm{mg\,m^{-2}}$. FESOM2.1–REcoM3 produces some outliers with up to $140\,\mathrm{mg\,m^{-2}}$ in the eastern Fram Strait. Complementing the regional summary, climatological maps of TChla are also included as Supplementary Fig. A2.

POC is assessed in regional box plots similar to Nöthig et al. (2020) in Fig. 3 panel b, where POC represents the sum of the particulate carbon pools in the model, i.e., phytoplankton carbon, detrital carbon, and carbon contained in TEP. Computed POC integrals for the upper 100 m ocean depth range from 0.2 to $18.6\,\mathrm{g\,C\,m^{-2}}$ (first to third quartile), with highest integrals in the Barents Sea between 6.0 and $15.1\,\mathrm{g\,C\,m^{-2}}$, and in the eastern Fram Strait with 4.7 to $18.6\,\mathrm{g\,C\,m^{-2}}$. As for TChla, intermediate

https://doi.org/10.5194/egusphere-2025-4190
Preprint. Discussion started: 4 October 2025

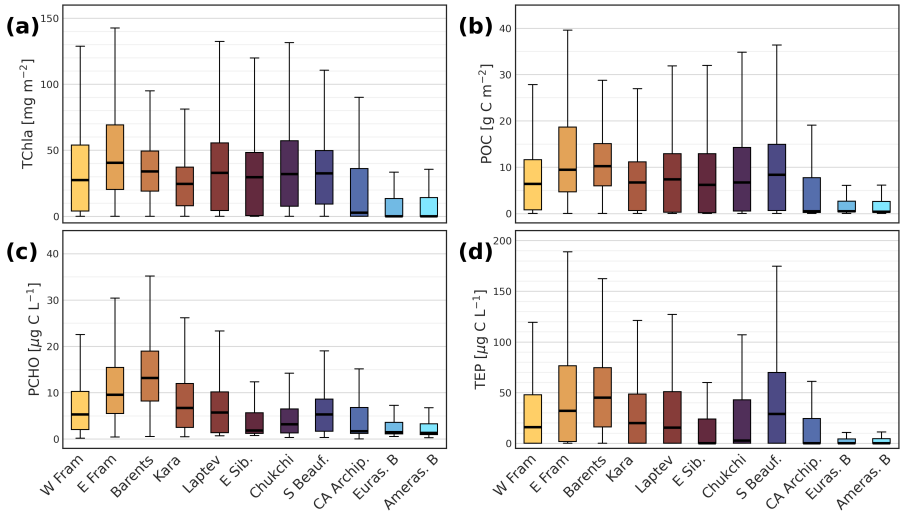

Figure 3. Box plots comparing regional differences for total Chlorophyll *a* (TChla, panel a), particulate organic carbon (POC, panel b), dissolved acidic polysaccharides (PCHO, panel c), and transparent exopolymer particles (TEP, panel d) following the region definitions mapped in Fig. 1 for western Fram Strait (W Fram, 10.8k data points), eastern Fram Strait (E Fram, 10.5k), Barents Sea (67.0k), Kara Sea (39.9k), Laptev Sea (21.2k), East Siberian Shelves (E Sib., 40.9k)), Chukchi Sea (25.6k), Southern Beaufort Sea (S Beauf., 9.7k), Canadian Archipelago (CA Archip., 62.9k), Eurasian Basin (Euras. B, 71.4k), and Amerasian Basin (Ameras. B, 112.8k). Data is averaged over May to September of 2000 to 2019, presented as depth integrals (0–100 m) for TChla and POC, and as volume-weighted mean (0–100 m) for PCHO and TEP. The thick black line represents the median, the box represents the first to third quartile. The whiskers span over 1.5 times the inter-quartile range.

levels of integrated POC (0.2–14.3 g C m^{-2}) are simulated for the western Fram Strait and on the shelves. In the central Arctic basins, the amount of integrated POC is low with 0.3 to 2.7 g C m^{-2}.

3.2 PCHO distribution in the Arctic

In this section, the production of PCHO is examined in relation to the phytoplankton bloom development. First, we analyze the regional long-term FESOM2.1–REcoM3 PCHO data as we did above for TChla and POC.Subsequently, the focus is directed particularly on the Fram Strait to assess the time evolution of phytoplankton blooming in comparison to PCHO production in a spatial context (Fig. 4). Finally, we present a seasonal cycle of phytoplankton TChla and carbon to show the organic carbon flux from photosynthesis towards particle formation in Fig. 5.

Regarding a regional overview in Fig. 3, PCHO concentration as volume-weighted mean over the upper 100 m is highest in the Barents Sea with a median of 13.15 µg C L^{-1}, while on the shelf seas, values of 1.8 to 7.0 µg C L^{-1} are computed (Fig. 3 panel c). The eastern Fram Strait PCHO median concentration of 9.5 µg C L^{-1} is higher than 5.3 µg C L^{-1} in the western Fram Strait. In contrast, much lower concentrations are obtained for the Eurasian and Amerasian Basin, where the median

https://doi.org/10.5194/egusphere-2025-4190
Preprint. Discussion started: 4 October 2025

ranges from 1.3 to 1.4 $\mu g\,C\,L^{-1}$. Climatological maps for 0–30 m volume-weighted mean concentration are presented in the Supplementary Fig. A2 to complement the regional overview.

To analyze the link between phytoplankton bloom evolution and PCHO production, the time period of May to July 2017 is chosen corresponding to the time of the PASCAL campaign and evaluated for SIC, DIN, TChla, and PCHO of the model's surface layer (0–5 m) in Fig. 4. In the northern Atlantic and Arctic Ocean, phytoplankton growth was mostly limited by light. Early in the season, sea ice covered most parts of the Arctic Ocean and Fram Strait. In contrast, the eastern Fram Strait was ice-free in May 2017 (Fig. 4 panel a). A phytoplankton bloom formed in the northern Atlantic and in the MIZ in the Fram Strait, most prominently along the ice edge (Fig. 4 panel g). This bloom shifted further north into the whole eastern Fram Strait in June, using up DIN. In the MIZ, a high TChla concentration of up to 6 $mg\,m^{-3}$ is simulated. In July, SIC decreased further and TChla concentrations of 2–7 $mg\,m^{-3}$ were found in the whole Fram Strait, with highest concentrations in the western part, and additionally in the northern Barents Sea of 2–5 $mg\,m^{-3}$ (Fig. 4 panels c and i, respectively). Simulated PCHO follows elevated TChla first northward and then westward in the Fram Strait area and reaches a surface concentration of up to 120 $\mu g\,C\,L^{-1}$ (Fig. 4 panels j–l), particularly when DIN is depleted (Fig. 4 panels d–f). In May, PCHO concentrations are most elevated close to the ice edge. In June, areas of elevated PCHO concentration are found towards the eastern Fram Strait and Barents Sea. In July, PCHO concentrations peak in the MIZ of the western Fram Strait and the northern Barents Sea alongside the phytoplankton blooms with 90 to 120 $\mu g\,C\,L^{-1}$.

The PASCAL campaign data of the same months in 2017 provides in situ measured concentrations of DCCHO in the open ocean, MIZ, and ice-covered regions around Svalbard. In situ concentrations were found to be lowest in the sea-ice leads within ice-covered regions ($11.3\pm10.1\,\mu g\,C\,L^{-1}$) and highest in the MIZ of $51.1\pm37.0\,\mu g\,C\,L^{-1}$. In the ice-free ocean, the mean measured DCCHO concentration was $17.2\pm5.2\,\mu g\,C\,L^{-1}$.

To assess the mean seasonal cycle over the years 2000 to 2019, phytoplankton carbon, TChla, PCHO, and TEP (the latter presented in detail in Sect. 3.3) concentrations are compiled as a volume-weighted mean of the upper 30 m of the ocean for the eastern Fram Strait (Fig. 5). The seasonal patterns of TChla and PCHO are evident in the climatology and similar to the results for 2017 shown in Fig. 4. The phytoplankton carbon concentration increases to peak at approximately 230 $\mu g\,C\,L^{-1}$ in July in line with the peak in TChla, with highest concentrations of 1.4 $mg\,TChla\,L^{-1}$. DIN concentration decreases from a winter average of about 3.5 $mmol\,m^{-3}$ with the start of the phytoplankton bloom in May to 0.5 $mmol\,m^{-3}$ in August. Following the bloom closely in time, PCHO is exuded by phytoplankton and its concentration rises to a maximum of approximately 50 $\mu g\,C\,L^{-1}$ in June. In the following months, PCHO concentration declines whereas TEP concentration rises quickly from May to July to 200 $\mu g\,C\,L^{-1}$, transferring the organic carbon from PCHO to TEP, and lagging approximately one month behind the peak of the phytoplankton bloom.

3.3 Occurrence of TEP in the Arctic

In this section, we first give an overview of the TEP simulation in the Arctic Ocean before describing the seasonal cycle with a focus on the Fram Strait, then broadening the perspective to an Arctic-wide climatology.

https://doi.org/10.5194/egusphere-2025-4190
Preprint. Discussion started: 4 October 2025

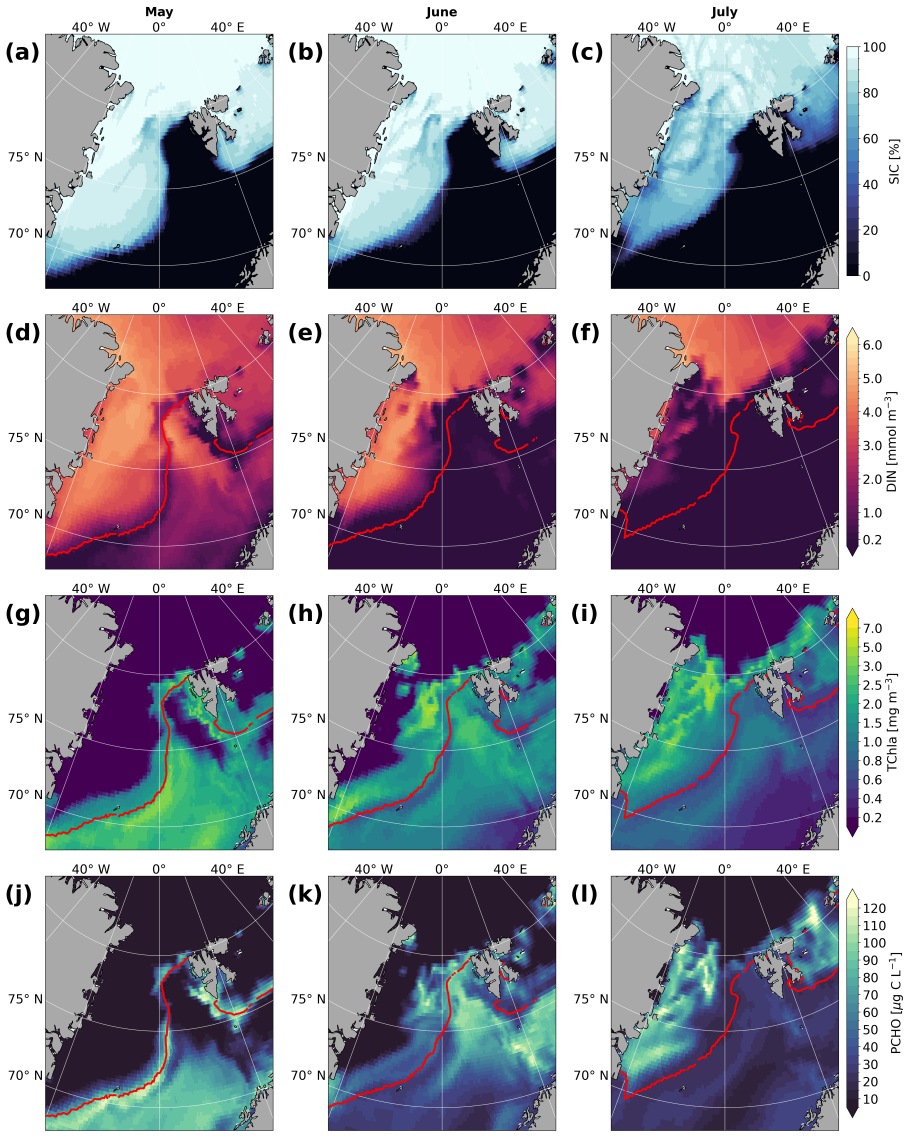

Figure 4. Maps of simulated sea-ice concentration (SIC, panel a–c), dissolved inorganic nitrogen (DIN, panel d–f), total Chlorophyll *a* (TChla, panel g–i) and dissolved acidic polysaccharides (PCHO, panel j–l) as monthly mean of May, June, and July 2017 for the model's surface layer (0–5 m). The contour of the sea-ice edge (defined as 25 % SIC) is depicted as red contour line.

As an overview, the TEP volume-weighted median concentrations of the upper 100 m of the water column are compiled as for PCHO in Fig. 3 panel d. Regional variations of TEP are high. The highest median of 44.9 µg C L^{-1} is reached in the Barents Sea. In the eastern Fram Strait, the median lies at 31.8 µg C L^{-1}, whereas in the western Fram Strait, Kara and Laptev Sea, median concentrations of 15.3–19.8 µg C L^{-1} are simulated. In the East Siberian and Chukchi Sea, as well as in the Eurasian

https://doi.org/10.5194/egusphere-2025-4190
Preprint. Discussion started: 4 October 2025

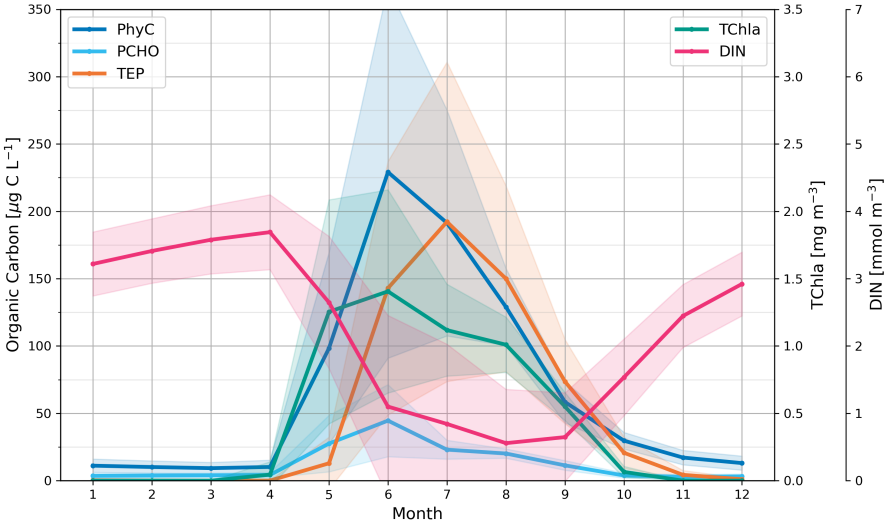

Figure 5. Seasonal cycle of simulated organic carbon concentration of phytoplankton (PhyC, blue, sum of small phytoplankton and diatom carbon), dissolved acidic polysaccharides (PCHO, cyan), and transparent exopolymer particles (TEP, orange) on the left axis; as well as total Chlorophyll *a* (TChla, teal) and dissolved inorganic nitrogen (DIN, magenta) concentrations on the right axis of the period 2000 to 2019 as volume-weighted mean of the upper 30 m ocean depth, averaged over the eastern Fram Strait (extent see Fig. 1). The standard deviation of each variable is computed from volume-weighted concentration across years and grid points in the regional subset and displayed as shaded area in corresponding colors.

and Amerasian Basin, median TEP concentration are below 3 µg C L^{-1}. Maximum simulated TEP concentrations reach nearly 190 µg C L^{-1} in the western Fram Strait.

The TEP concentration exhibits a phase-shifted seasonal cycle following the phytoplankton bloom in the eastern Fram Strait area (Fig. 5). It is close to zero during winter months and starts to rise in early May, lagging approximately one month behind the TChla and phytoplankton carbon concentrations. It peaks at 150 µg C L^{-1} in August and quickly declines thereafter.

For the Arctic-wide context, monthly climatological maps of TEP are provided for April to November as a volume-weighted mean of 0–30 m (Fig. 6). In May, TEP concentrations rise first in regions with phytoplankton blooms (c.f. monthly climatology of TChla and PCHO in the Supplementary Fig. A2, i.e., in the Fram Strait and on the continental shelves (50–150 µg C L^{-1}). The climatology further shows that from June to August, TEP increase in the Fram Strait, on the Siberian shelves, in the Chukchi and Beaufort Seas, reaching approx. 200–400 µg C L^{-1}. The mean concentration in the central Arctic Ocean reaches 10–50 µg C L^{-1} in the upper 30 m of the water column. There is a gradient of TEP from the shelves towards the Arctic Ocean basins during summer in the simulation. Beginning in September, TEP declines in the whole Arctic region. TEP is then remineralized or sinks to deeper ocean layers, and surface concentrations decline.

https://doi.org/10.5194/egusphere-2025-4190
Preprint. Discussion started: 4 October 2025

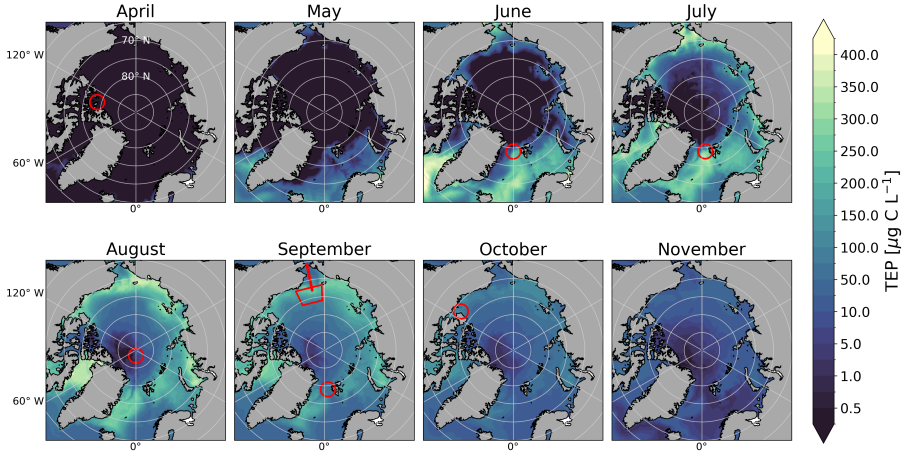

Figure 6. Climatological maps of transparent exopolymer particles (TEP) concentration as volume-weighted mean of the upper 30 m of the simulated period 2000 to 2019. Overlaid are the positions of the observation data points in red (c.f. Tab. 5).

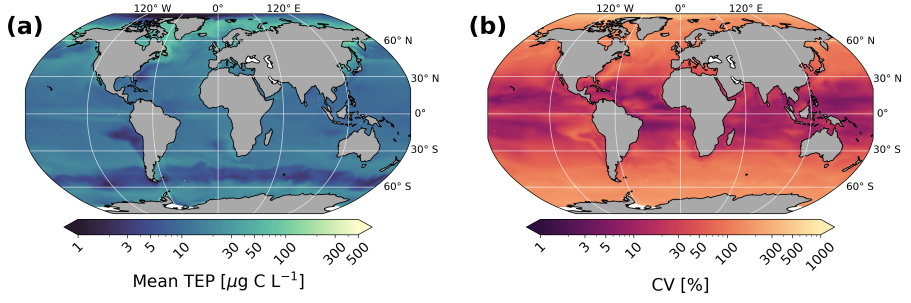

Figure 7. Maps of global transparent exopolymer particle (TEP) concentration as volume-weighted mean (0–30 m) of the years 2000 to 2019 (panel a) and its coefficient of variation (panel b). The coefficient of variation is computed for each grid point across years based on volume-weighted concentrations.

3.4 Global TEP patterns

As detailed in Sect. 2.1, the FESOM2.1–REcoM3 setup used in this study is optimized in its parameterization and irregular grid to enable reliable Arctic eddy-permitting simulations of PCHO and TEP. However, since FESOM2.1–REcoM3 is a global model in principle, we additionally evaluate the TEP concentration relative to its global pattern. Because in situ observations are available mostly for surface waters (reviews by Wurl and Cunliffe, 2017; Zamanillo et al., 2019), the model results are presented here as volume-weighted mean of the upper 30 m of the ocean averaged over 2000 to 2019. For completeness, global model results of TChla and PCHO can be found as Supplementary Fig. A3. Furthermore, mean TEP concentrations are also summarized by binning for each Longhurst Provinces (Longhurst, 2006), presented as Supplementary Tab. A2.

https://doi.org/10.5194/egusphere-2025-4190
Preprint. Discussion started: 4 October 2025

In large areas of the global ocean, simulated TEP concentration in FESOM2.1–REcoM3 ranges from 5 to 50 $\mu g\,C\,L^{-1}$ (Fig. 7, panel a). TEP concentrations are especially high in the Nordic Seas and the Arctic Ocean with approx. 75 to 150 $\mu g\,C\,L^{-1}$. In the region of the Antarctic Polar Front and in the Peruvian upwelling, TEP concentrations reach a minimum below 5 $\mu g\,C\,L^{-1}$. The coefficient of variation of monthly, volume-weighted mean TEP concentration is highest in the Arctic region north of 75° N with up to 800 %, while between 30° S to 30° N, the coefficient of variation is lowest with less than 30 % (Fig. 7 panel b). In the Southern Ocean, the coefficient of variation ranges from 100 to 200 %.

4 Evaluation and interpretation

We integrated, tested and analyzed a TEP parameterization in a state-of-the-art global ocean biogeochemistry model, the third version of the Regulated Ecosystem Model (REcoM3; Gürses et al., 2023) coupled to the Finite volumE Sea-ice Ocean circulation Model (FESOM2.1; Danilov et al., 2017). The newly introduced scheme is based on the TEP aggregation model developed by Engel et al. (2004) and Schartau et al. (2007). The simulation results of FESOM2.1–REcoM3 of phytoplankton biomass were presented together with the organic carbon exudation and aggregation products, first and foremost for the Arctic Ocean and also briefly for the global ocean.

In the following, the model performance is evaluated by comparing the Arctic phytoplankton distribution in terms of TChla and POC with remote sensing and available in situ datasets (Sect. 4.1) as a foundation for the analysis of exuded PCHO (Sect. 4.2) and its aggregation to TEP (Sect. 4.3). This discussion is ordered by regions and available observational studies, which are unfortunately widely spread across different years and regions. It partly focuses on examining the bloom phenology in the Fram Strait as an example of a data-rich region. As a last step, the globally simulated TEP concentration is contextualized with observational data (Sect. 4.4).

4.1 Simulated phytoplankton distribution in the Arctic Ocean

In terms of Arctic-wide TChla, the FESOM2.1–REcoM3 output aligns with the compiled remote-sensing data of CMEMS TChla. However, in the inner shelf areas (the Barents, Kara, and Laptev Seas and close to the Canadian coast) FESOM2.1–REcoM3 shows much lower concentrations (Fig. 2 panel a), whereas in the Chukchi and Beaufort Seas, and western Fram Strait, FESOM2.1–REcoM3 shows higher TChla than CMEMS. One explanation for the observed difference may be that CMEMS sampled far less days than are simulated by FESOM2.1–REcoM3. Schourup-Kristensen et al. (2018) explain lower TChla in the simulation by full spatial and temporal coverage whereas only open-water productive regions are accessible from remote-sensing measurements. Additionally, CMEMS is error-prone on large parts of the Arctic shelves, most likely due to the very high colored dissolved organic matter and total suspended matter concentrations, which have not been sufficiently accounted for in the retrieval process. This results in a significant overestimation of TChla (Copernicus Marine Service, 2023; Heim et al., 2014; Schourup-Kristensen et al., 2018). Also other remote-sensing products overestimate TChla on the Arctic shelves (Mustapha et al., 2012). In the Chukchi and Beaufort Seas, the simulated TChla concentration itself (and the difference between FESOM2.1–REcoM3 and CMEMS) is low (less than 1.5 $mg\,m^{-3}$, Fig. 2 panel c). Other observations from in situ

https://doi.org/10.5194/egusphere-2025-4190
Preprint. Discussion started: 4 October 2025

data and satellite-derived products draw a diverse picture in these seas with massive under-ice blooms in the Chukchi Sea with high TChla concentration of up to 30 $\mathrm{mg\,m^{-3}}$ (Arrigo et al., 2014), and low (0.02–0.25 $\mathrm{mg\,m^{-3}}$) TChla concentration in the northern Chukchi and Beaufort Seas (Jung et al., 2022; Park et al., 2019).

Comparing FESOM2.1–REcoM3 to the Arctic TChla product presented in Lewis et al. (2020), the agreement is similar as with the CMEMS product, but the spatial patterns are very different (Supplementary Fig. A1). This satellite product shows even lower TChla concentration in large parts of the Arctic but agrees better with the simulation in the southern Barents Sea and Laptev Sea shelf break where TChla is still higher with reaching maximum values of 7 $\mathrm{mg\,m^{-3}}$. Lewis et al. (2020) derive TChla estimates by applying different retrieval parameters in different regions, as developed by Lewis and Arrigo (2020). This leads to a good fit to in situ measurements but produces abrupt changes in TChla estimates across region boundaries. The choice of methods (CMEMS compared to Lewis et al., 2020) profoundly impacts the remote-sensing products. As such, priority is given to the CMEMS Arctic TChla product as it is more consistent across the whole Arctic Ocean, despite overestimation on the inner shelves (Copernicus Marine Service, 2023).

With regard to in situ measurements of TChla, the FESOM2.1–REcoM3 simulation compares well to the results from Nöthig et al. (2020) and also to other observations. In the eastern Fram Strait, in situ measurements of Nöthig et al. (2020) result in a median vertically integrated concentration of 44 $\mathrm{mg\,m^{-2}}$ (0–100 m depth), and in the Barents Sea of 42 $\mathrm{mg\,m^{-2}}$ which agree with simulated median concentrations of 40.4 and 33.8 $\mathrm{mg\,m^{-2}}$, respectively (Fig. 3 panel a). The results are also in line with the two-year round mooring observations at the long-term ecological research observatory HAUSGARTEN in the eastern Fram Strait with simulated TChla concentration reaching up to 5 $\mathrm{mg\,m^{-2}}$ in the upper 30 m compared to 7 $\mathrm{mg\,m^{-2}}$ in measurements (von Appen et al., 2021). In the MIZ, especially in the area of Fram Strait, phytoplankton growth is expected to be highest, as the sea-ice breaks up, light availability is increased and the water column is stratified (Cherkasheva et al., 2014; Nöthig et al., 2020).

Likewise in the western part of Fram Strait and in the Siberian seas, the lower amount of simulated TChla matches in situ data for these regions spanning 13 to 26 $\mathrm{mg\,m^{-2}}$ (Nöthig et al., 2020; Piontek et al., 2021). Vertically integrated TChla is even lower in the Arctic Ocean basins in both simulation (integrated over 0–100 m water depth, median 0.01 $\mathrm{mg\,m^{-2}}$) and measurements (7–8 $\mathrm{mg\,m^{-2}}$). A likely explanation for the higher computed median TChla concentration in several regions and higher variability in comparison to Nöthig et al. (2020) might be the consideration of up to 62k data points in the regional subsets (Fig. 3 panel a) compared to only a few hundred in Nöthig et al. (2020), where the in situ sampling is mostly limited to one campaign each spring-summer season. Furthermore, the evaluated regions contain the whole continental shelve grid points, whereas the in situ measurements are located mostly in the northern parts of the shelf seas. Climatological maps of TChla are included as Supplementary Fig. A2.

Similar to TChla, simulated POC is assessed in regional overviews (Fig. 3 panel b). These are generally in agreement with the observations of Nöthig et al. (2020), who also measured the highest vertically integrated median POC concentration of 13 $\mathrm{g\,C\,m^{-2}}$ in the eastern Fram Strait (integrated over 0–100 m water depth). Also, Engel et al. (2019) found approx. 16 $\mathrm{g\,C\,m^{-2}}$ POC in the eastern Fram Strait over 2009 to 2017, comparable to a median POC concentration of 9.5 $\mathrm{g\,C\,m^{-2}}$ in FESOM2.1–REcoM3. Regarding the western Fram Strait and the Siberian shelves, the simulation yields higher vertically

https://doi.org/10.5194/egusphere-2025-4190
Preprint. Discussion started: 4 October 2025

integrated median concentrations (6.2–10.2 $\mathrm{g\,C\,m^{-2}}$) at spatio-temporal measurement locations of Nöthig et al. (2020), i.e., 5–8 $\mathrm{g\,C\,m^{-2}}$). The higher simulated POC on the shelves might be caused by including also southern shelf regions with higher POC concentration into the median calculation, whereas the measurements do not cover these areas. With respect to the central Arctic, Nöthig et al. (2020) estimated the interquartile range of vertically integrated POC concentration to 1 to 8 $\mathrm{g\,C\,m^{-2}}$ from their long-term observations in the Eurasian Basin, while Piontek et al. (2021) provide data on POC of approx. 3 to 5 $\mathrm{g\,C\,m^{-2}}$ in the Eurasian Basin in 2012, which are on the same order of magnitude as the simulated vertically integrated POC concentration of 0.4 to 2.7 $\mathrm{g\,C\,m^{-2}}$ interquartile range in the present analysis.

4.2 PCHO and its link to phytoplankton blooms

Based on a reasonable agreement of the simulation in terms of TChla and POC laid out, the focus is now directed towards the evaluation of the PCHO implementation into FESOM2.1–REcoM3. There is only a limited amount of observational data available to discuss the simulation of PCHO in the Arctic. As such, the model results in the Fram Strait are singled out along with the DCCHO dataset of the PASCAL campaign in 2017, before the perspective is broadened to the few studies in the other Arctic regions.

Focusing on the Fram Strait area in the single year 2017, there is a reasonable agreement with the PASCAL campaign data of the same summer months, assuming that the simulated PCHO reflects most of the DCCHO pool (Methods Sect. 2.5). The MIZ exhibits the highest concentrations in both measurement and simulation. In general, in FESOM2.1–REcoM3, the regions of elevated PCHO follow the phytoplankton bloom patterns. Interestingly, there is a case in the simulation, where high TChla does not result in high PCHO concentration: in June in the south-western Fram Strait (Fig. 4 panel k). The carbon overflow hypothesis probably offers an explanation (Engel et al., 2004, 2020): DIN has not been used up completely in this area; hence, the phytoplankton are not experiencing nutrient depletion. The implemented limiter function for phytoplankton carbon exudation (depending on the intracellular N:C ratio, Eq. 5) is apparently still low, and as such, the phytoplankton cells are not exuding much excess carbon.

In the eastern Fram Strait, von Jackowski et al. (2020) observe DCCHO in concentrations of 55.8 $\mathrm{\mu g\,C\,L^{-1}}$ in July and 22.5 $\mathrm{\mu g\,C\,L^{-1}}$ in September (0–100 m), which are slightly higher than the FESOM2.1–REcoM3 summer PCHO median (Fig. 3 panel c). Comparable to the simulation, the DCCHO concentration is significantly correlated to TChla in their study. Regarding other regions in the Arctic, the model results are in the same order of magnitude as observations by Piontek et al. (2021) in the Eurasian Basin, the northern Barents Sea, and northern Laptev Sea. Piontek et al. (2021) measured 25.5–30.8 $\mathrm{\mu g\,C\,L^{-1}}$ DCCHO in the upper 40 m in August to October 2012 compared to 10–80 $\mathrm{\mu g\,C\,L^{-1}}$ of PCHO in this analysis (Supplementary Fig. A2). In the Eurasian Basin, Gao et al. (2012) report 88–502 $\mathrm{\mu g\,C\,L^{-1}}$ DCCHO in August for the upper ocean (0.5 m) during a drift campaign in a re-freezing lead. These observations show higher concentrations than results presented here, but it is difficult to compare the FESOM2.1–REcoM3 simulation with bulk measurements for the upper five meter of the water column. Additionally, the authors attribute the high DCCHO to the exudation of DCCHO due to the freezing conditions and not to nutrient stress.

https://doi.org/10.5194/egusphere-2025-4190
Preprint. Discussion started: 4 October 2025

At greater depths, there is a steep decline in simulated PCHO concentration. Piontek et al. (2021) also report a decreasing DCCHO concentration with depth for the Eurasian Basin similar to, though less pronounced than in, the simulation. The volume-weighted median of 0–100 m depth of PCHO in FESOM2.1–REcoM3 drops to 1.3 µg C L^{-1} (Fig. 3 panel c), while approx. 19–23 µg C L^{-1} DCCHO in the depth range 40 to 150 m are reported by Piontek et al. (2021). This discrepancy might be caused by the specific timing of the campaign during a year with an extraordinarily low sea-ice concentration, which led to high TChla and a strong nutrient depletion, to which Piontek et al. (2021) relate the high amounts of exuded DCCHO. Overall, the simulated PCHO concentration clearly underlines the link of high PCHO to high TChla concentrations coinciding with nutrient depletion in the open ocean and in the MIZ (e.g., July 2017 in West Fram Strait, Fig. 4). Furthermore, the simulation results show that PCHO largely does not accumulate in the upper ocean, but quickly aggregates to TEP (Fig. 5).

4.3 TEP in the surface waters of the Arctic Ocean

Throughout the year, TEP concentrations rise with the beginning of summer and decline quickly in autumn (Fig. 5). The highest concentrations are simulated along the coastline and with a decrease towards the central Arctic Ocean. Yamada et al. (2015) highlight this TEP concentration gradient in their study on the Chukchi shelf and Canadian basin (shelf 138.9±64.7 µg C L^{-1} to slope/basin: 79.3±15.5 µg C L^{-1}, 0–50 m) and attribute it to TChla co-occurrence, transport from the shelf towards the basin, and additional TEP production by prokaryotes. Further, the TEP seasonality is in accordance with TEP observations of von Jackowski et al. (2020) revealing a strong decline from summer to autumn (observation of 21.4±14.5 µg C L^{-1} in July, 7.1μ5.2 µg C L^{-1} in September, 0–100 m, compared to simulated 76.10±50.68 µg C L^{-1} in July, 27.81±14.51 µg C L^{-1} in September), which the authors link to remineralization and sinking as larger particles out of the water column. In the compiled climatology for the eastern Fram Strait, TEP concentration lags approximately one month behind the TChla increase and decrease.

From 2017 data, it is concluded that TChla alone is not a good predictor for TEP concentration. The release of PCHO as TEP-predecessor depends also on the nutrient stress of phytoplankton (Fig. 4), and as such, the model setup is in agreement with the carbon overflow hypothesis (Engel et al., 2004, 2020). Furthermore, Engel et al. (2017) reported a strong link between TEP and *Phaeocystis spp.* occurrence patterns in the Fram Strait region. With respect to this phytoplankton species, also Zamanillo et al. (2019) found TEP concentration positively correlated to phytoplankton biomass along a wide transect in the Atlantic Ocean. The setup of FESOM2.1–REcoM3 includes only diatoms and small phytoplankton as distinct groups with—so far— similar implementation of carbon exudation. Here, the recent developments of REcoM3 towards including additional phytoplankton functional groups (Seifert et al., 2022) could help to distinguish contributions of different phytoplankton functional groups to carbon exudation.

Regarding the Arctic-wide occurrence of TEP, the available observations are very limited in space and time. Each measurement depends on a very local set of ecological conditions shaping sea ice concentration, nutrient availability, and phytoplankton blooms. These in situ observations are compared to monthly integrated simulation results for a small area enclosing the corresponding observation location in Tab. 5, complementary to the maps of simulated TEP concentration in Fig.6. Overall, there is a fairly good agreement of the simulated TEP concentration to in situ observations with a correlation coefficient of 0.71

https://doi.org/10.5194/egusphere-2025-4190
Preprint. Discussion started: 4 October 2025

Table 5. Comparison of carbon concentration of transparent exopolymer particles (TEP) of observational campaigns and simulation. Model results are volume-weighted and averaged corresponding to the depth range, area, and month of observations. To best fit the spatial extent of in situ measurements, a latitude-longitude box was defined on the model grid for each observation, resulting in a variable number of model grid cells included in the calculation. Mean and standard deviation of the years 2000 to 2019 are stated in brackets. References of measurements refer to Wurl et al. (2011, W2011), Engel et al. (2020, E2020), von Jackowski et al. (2020, vJ2020), Olli et al. (2007, O2007), and Yamada et al. (2015, Y2015)

Period	Region	Depth [m]	Modeled TEP [µg C L^{-1}]	Observed TEP [µg C L^{-1}]	Number of grid cells	Reference
Mar-Apr 2010	Catlin Ice Base	0–14	0±0 (0±0)	405.9±344.7	65	W2011
Jun 2015	Fram Strait	5–200	16.0±11.3 (20.9±16.6)	8.2±6.1	935	E2020
Jul 2018	Fram Strait	0–100	102.9±23.5 (88.4±35.3)	21.4±14.5	1631	vJ2020
Aug 2001	Eurasian Basin	0–200	0.002±3e-51 (0.6±1.6)	31.0–37.0	135	O2007
Sep–Oct 2018	Fram Strait	0–100	32.3±7.5 (27.7±11.6)	7.1±5.2	2440	vJ2020
Sep–Oct 2012	Chukchi Shelf	0–50	115.3±72.6 (77.5±46.9)	138.9±64.7	1106	Y2015
Sep–Oct 2012	Canada Basin	0–200	29.2±6.9 (23.8±11.0)	70.4±15.5	14940	Y2015
Oct 2009	NW Passage	0–29	137.0±12.1 (108.0±33.0)	126.1±69.7	174	W2011

($p = 0.11$, see also Supplementary Fig. A4), despite the modeled TEP concentrations being often slightly higher and differing particularly in the region of the Catlin Ice Base in the Canadian Arctic Archipelago. Here, Wurl et al. (2011) obtained their measurements from an under-ice phytoplankton bloom, which resulted in very high production of TEP. Such an event is not reproducible by FESOM2.1–REcoM3 because ice-algae are not explicitly modeled, and light-through-ice transmission is not adequately represented. Similarly in the Central Arctic Ocean, Olli et al. (2007) conducted a drift experiment measuring TEP concentration in the pack ice. The authors found a uniform depth distribution of TEP along the drift track, which could be supplied by the continuous primary production in the upper water column in open leads and melt ponds. However, there is nearly no TEP simulated in this area by FESOM2.1–REcoM3. The absence could originate from the missing under-ice or ice-algae production in the model, which have been part of other modeling approaches (e.g., Castellani et al., 2017).

https://doi.org/10.5194/egusphere-2025-4190
Preprint. Discussion started: 4 October 2025

Overall, it has been shown that FESOM2.1–REcoM3 is capable of simulating the TEP distributions in the Arctic Ocean well. As this is a first step to simulate TEP in the Arctic Ocean, the full complexity of TEP cycling is not yet represented in the model parameterization. Wurl et al. (2011) provide a conceptual model of TEP dynamics, of which only the exudation of organic carbon, its aggregation and TEP formation, and the remineralization are implemented in this simulation. Other processes of the life cycle of TEP, such as TEP ballasting by other particles, and sinking in the water column, or microbial/ zooplankton grazing on TEP, have not yet been implemented (Wurl et al., 2011). Additionally, Galgani et al. (2016) describe high concentrations of TEP and its precursors in melt ponds and in leads in the central Arctic Ocean and argue that TEP could also be released from melting sea ice. This would require a more sophisticated implementation of the sea-ice compartment in FESOM2.1–REcoM3. Zampieri et al. (2021) have already coupled FESOM2 with the model Icepack, providing more detailed sea-ice physics but also increased model complexity and cost. Another categorical light-through-ice transmission approach was suggested by Castellani et al. (2017), both could offer valuable perspectives for improved representation of under-ice algae blooms and therefore, also of PCHO and TEP.

The peak concentration of TEP in FESOM2.1–REcoM3, especially regarding the ocean surface, might be too high. One reason might be that in the current implementation, TEP aids in the aggregation of other particles (the TEP dependency of the aggregation rate, Eq. 7), but is not itself transferred in the process. Another reason could be the missing transfer of particles into the surface microlayer and an enrichment there. The surface microlayer is the very thin transition film at the ocean–atmosphere interface, which is not part of the model structure. TEP was reported to be positively buoyant when not ballasted by other minerals or particles, thus, TEP would ascend through the water column and become enriched in this layer (Azetsu-Scott and Passow, 2004; Wurl et al., 2011). In a methodological study, Robinson et al. (2019) demonstrate the enrichment of TEP via bubble scavenging, a process by which rising air bubbles transport organic matter. Observational studies report contrasting results on surface microlayer enrichment: Galgani et al. (2016) report only a minor enrichment in the surface microlayer in the open water of the central Arctic, whereas Wurl et al. (2011) calculated an enrichment factor of 1.7 ± 0.5 in the Canadian Arctic. Two obstacles make it difficult to simulate the surface microlayer. Firstly, incorporating such a thin layer in a global ocean model is challenging due to numerical constraints. In FESOM2.1–REcoM3, the upper ocean is only resolved as layers spanning five meter depth. Secondly, the complexity of processes in the surface microlayer is difficult to capture. It would be necessary to consider the physical interactions at the air–sea interface and a different balance of the biogeochemical processes (microorganisms, gel phases, aerosol formation; Engel et al., 2017) compared to the underlying bulk water.

Regarding the carbon export to the deep ocean in FESOM2.1–REcoM3, there are two detritus classes sinking with either increasing speed with depth (following Kriest and Oschlies, 2008) or constant, fast sinking mimicking zooplankton fecal pellets (Karakuş et al., 2021). Regarding TEP, no explicit sinking has been implemented in the model because of its positive buoyancy. Still, the FESOM2.1–REcoM3 simulation contains a substantial decrease of TEP concentration with depth alongside the phytoplankton biomass decrease with depth. There are several aspects to consider for the addition of a TEP sinking parametrization: Firstly, Iversen and Lampitt (2020) report that there is often no correlation between particle size and sinking speed. Similarly, Chajwa et al. (2024) have recently discovered a matrix of organic carbon forming around TEP, which slows down the sinking considerably in the water column. Secondly, there is a degradation of particular and dissolved organic mat-

https://doi.org/10.5194/egusphere-2025-4190
Preprint. Discussion started: 4 October 2025

ter which is regarded as ecosystem-dependent, especially concerning the specific microbial community engaged in turnover processes (Levine and DeVries, 2024). Additionally, the explicit representation of the heterotrophic microbial community in a global ocean model suggests that environmental conditions impact the degradation of dissolved organic matter, predominantly by nutrient limitation of heterotrophs in the upper ocean and carbon limitation in the deep ocean (Lennartz et al., 2024). These aspects represent ongoing research on the link between the upper ocean and the export of organic carbon to greater depths, also called the biological carbon pump. The cited studies provide insight into the diverse and complex biogeochemical processes that warrant consideration, underscore the prevailing analytical uncertainties, and point out the need for reassessment of particle sinking speed and organic matter degradation. As a result, there is a need to revisit the carbon sequestration estimates for the global ocean (Iversen, 2023). Therefore, the development of FESOM2.1–REcoM3 to explicitly resolve the sinking of TEP through the water column and to provide a detailed account of the degradation processes could lead to a more realistic representation of TEP in the Arctic and the global ocean. To date, most Earth System Models have not fully incorporated these processes, resulting in significant uncertainty regarding estimates of the biological carbon pump in response to climate change (Henson et al., 2022; Wilson et al., 2022). It is anticipated that further advances in the observational understanding of particle sinking and the biological carbon pump, along with their incorporation into model parameterization, may lead to an updated quantification of carbon export.

The observational caveats of this analysis include the scarcity of sampling campaigns, the broad spatial and temporal gaps inbetween studies, and their differences in sampling depths and methodologies (listed in Tab. 5). These make it difficult to construct consistent time series for biogeochemical parameters from observational studies, which therefore limit the model evaluations. At least for the Fram Strait, there is a valuable in situ time series on TChla and POC (Nöthig et al., 2020), which is complemented by DCCHO and TEP measurements in the recent years (Engel et al., 2017, 2020; von Jackowski et al., 2020). Several studies provide campaign data repeatedly from areas within the pack ice in the high Arctic of marine organic carbon particles and their transfer from the ocean into the atmosphere (Gao et al., 2012; Lawler et al., 2021; Orellana et al., 2011). Ideally, the measurement campaigns at these locations—as examples for regions with varying sea-ice conditions and year-round ice coverage—should be extended by DCCHO and TEP sampling in the upper ocean, and as such, be continued to infer long-term trends. This can also help to distinguish between the ice-algae or pelagic phytoplankton release of organic carbon. Additionally, further studies should provide nutrient measurements alongside DCCHO determination in order to foster understanding of phytoplankton carbon exudation as postulated by the carbon overflow hypothesis (Engel et al., 2004, 2020) in different Arctic environments. This could also enable a model refinement with phytoplankton group-specific PCHO exudation ratios or their time-dependencies during different phases of the bloom.

4.4 TEP occurrence in the global ocean

Engel et al. (2020) propose three different ocean regimes of TEP occurrence, to which the model results are compared: an oligotrophic regime, a polar regime, and an eastern boundary upwelling regime. The first, oligotrophic regime, is characterized by low phytoplankton productivity, which also results in low TEP concentrations. In large parts of the Atlantic, Pacific, and Indian Ocean, the simulated annual mean TEP concentration ranges between 5 and 25 $\mu g\,C\,L^{-1}$ (Fig. 7). This agrees with in

https://doi.org/10.5194/egusphere-2025-4190
Preprint. Discussion started: 4 October 2025

situ data: Data reviewed in Zamanillo et al. (2019) show the same concentration range of 5 to 36 $\mu g\,C\,L^{-1}$. Furthermore, in the tropical Atlantic, the observed TEP concentration is also low at approximately 5–10 $\mu g\,C\,L^{-1}$ (Engel et al., 2020; Wurl and Cunliffe, 2017).

According to Engel et al. (2020), within the second regime represented by the polar regions, TEP accumulates in the upper ocean layer. The authors attribute this mainly to the occurrence of the phytoplankton *Phaeocystis spp.* and microbial degradation focusing primarily on proteinaceous compounds rather than on TEP, while Wurl et al. (2011) observed diatom bloom dominance at their Arctic stations. For the Arctic Ocean, the simulated strong seasonality of TEP is discussed above (Sect. 4.3). In the Southern Ocean during the blooming period between December and March, simulated TEP concentrations increase to approximately 10–150$\mu g\ C\ L^{-1}$, agreeing well to observational studies reporting 0–39 $\mu g\,C\,L^{-1}$ in the open waters of the Southern Ocean (Engel et al., 2020; Wurl and Cunliffe, 2017). In the coastal waters, even higher TEP concentrations are measured of approximately 200 $\mu g\,C\,L^{-1}$ in Bransfield Strait (Corzo et al., 2005 reviewed in Wurl and Cunliffe, 2017).

As a third regime, the eastern boundary upwelling systems are described as highly productive regimes, which also results in high TEP production and fast particle sinking because of ballasting (Engel et al., 2020). The authors report TEP concentration of up to 85 $\mu g\,C\,L^{-1}$ in the Mauritanian, but only 9 $\mu g\,C\,L^{-1}$ in the Peruvian upwelling system, which they attributed to high grazing rates by zooplankton and heterotrophic consumption. High TEP amounts of up to 1200 $\mu g\,C\,L^{-1}$ are reported for the California Current (Zamanillo et al., 2019). In the Arctic configuration of FESOM2.1–REcoM3 used here, these eastern upwelling regions are not sufficiently resolved, and as a consequence, have a primary production that is too low and thus, lack the phytoplankton carbon exudation and the resulting high TEP concentrations.

Overall, the simulated global TEP patterns are in good agreement with observational studies when the phytoplankton blooms are simulated successfully (Fig. 7 on TEP and Supplementary Fig. A3 on TChla). This study is a first step of modeling TEP in a large-scale ocean biogeochemistry model.

5 Conclusions

In this study, we assess the two-size class parameterization of dissolved acidic polysaccharides (PCHO) and transparent exopolymer particles (TEP) (below and above 0.4 μm) proposed by Engel et al. (2004) in the Arctic setup of the coupled ocean circulation biogeochemistry model FESOM2.1–REcoM3 (Oziel et al., 2025). The main advantage of FESOM2.1–REcoM3 lies in its flexible phytoplankton stoichiometry allowing for carbon overflow under nutrient-depleted conditions. Additionally, FESOM2.1–REcoM3 profits from its thorough evaluation in a wide range of applications (Friedlingstein et al., 2023; Gürses et al., 2023; Hauck et al., 2020; REcoM only: Laufkötter et al., 2015, 2016; Tagliabue et al., 2016), including an Arctic-specific setup (Oziel et al., 2025, 2022; Schourup-Kristensen et al., 2014, 2018, 2021). This allows the explicit simulation of nutrient limitation and carbon overflow within the two implemented phytoplankton classes, along with the estimation of PCHO and TEP formation in the Arctic Ocean.

The results of the current setup agree reasonably well with in situ and remote-sensing measurements of phytoplankton biomass in terms of TChla and POC. Despite the simplifications involved in implementing PCHO formation as a fraction

https://doi.org/10.5194/egusphere-2025-4190
Preprint. Discussion started: 4 October 2025

of exuded organic carbon, aggregation to TEP, and their remineralization, we demonstrate that the use of this parameterization resulted in a simulation of spatial and seasonal dynamics of TEP concentration in the Arctic, which closely follows the phytoplankton blooms. The simulated PCHO and TEP concentrations compare reasonably well to in situ observations.

Our study presents the first Arctic-adapted high-resolution simulation of TEP in a global setup. Despite well-recognized limitations in reproducing fine-scale TEP dynamics, this approach facilitates the provision of first-order estimates of the magnitude, timing, and sensitivity of TEP at the pan-Arctic scale. In particular, it highlights the need to collect more in situ observations. At present, the limited amount of observations hampers further improvement and evaluation of such parameterizations. Nevertheless, this analysis paves the way for considering TEP in Earth System Models and for research on the link of dissolved and particulate organic carbon to marine biogenic aerosol precursors (Leon-Marcos et al., 2025). Perspectively, this model approach can also contribute to the assessment of the impact of biogenic aerosol precursors on the Arctic atmosphere in the context of climate change.

Code and data availability. The FESOM2.1–REcoM3 code including the implementation of TEP, the model grid, and the curated simulation results are available at https://doi.org/10.5281/zenodo.15174190 (Zeising et al., 2025). In general, FESOM2.1–REcoM3 model source code is steadily updated and accessible at https://github.com/FESOM/fesom2. The grid *fARC* is also provided at the official FESOM site at https://gitlab.awi.de/fesom/farc. The evaluation of model output was done using python3.13 (Python Software Foundation) and the modules *pyfesom2* (https://github.com/FESOM/pyfesom2) and *py_f2recom* (not published, MarESys group, AWI), which are based on *xarray*, *scipy*, *cartopy*, and *matplotlib*, among others.

Observation data sets for model evaluation were obtained directly from the cited literature. The Copernicus Marine Environment Monitoring Service level 4 monthly reprocessed Ocean Color product (Product ID: OCEANCOLOUR_ARC_BGC_L4_MY_009_124) was obtained from Copernicus Marine Data Store at https://data.marine.copernicus.eu/product/OCEANCOLOUR_ARC_BGC_L4_MY_009_124/. The Arctic Ocean TChla product presented in Lewis and Arrigo (2020) was downloaded from Stanford Digital Repository at https://doi.org/10.25740/kc822vj3040. The DCCHO data set used in von Jackowski et al. (2020) is published at https://doi.pangaea.de/10.1594/PANGAEA.915751. The DCCHO data set of Zeppenfeld et al. (2023a) from the PASCAL campaign on RV *Polarstern* is available at https://doi.pangaea.de/10.1594/PANGAEA.961004. The Longhurst provinces were provided as shapefiles by marineregions.org (Flanders Marine Institute, 2009).

https://doi.org/10.5194/egusphere-2025-4190
Preprint. Discussion started: 4 October 2025

Appendix A: Supplementary tables and figures

https://doi.org/10.5194/egusphere-2025-4190
Preprint. Discussion started: 4 October 2025

Table A1. List of abbreviations.

Abbreviation	Description
CMEMS	Copernicus Marine Environment Monitoring Service level 4 monthly reprocessed Arctic Ocean Color product
DCCHO	Dissolved Combined Carbohydrates
DIC	Dissolved Inorganic Carbon
DIN	Dissolved Inorganic Nitrogen
DOC	Dissolved Organic Carbon
FESOM	Finite VolumE Sea-ice Ocean Model
MIZ	Marginal Ice Zone
NPP	Net Primary Production
PASCAL	Physical feedbacks of Arctic Boundary Layer Sea ice, Cloud And Aerosol campaign
PCHO	Dissolved Acidic Polysaccharides
REcoM	Regulated Ecosystem Model
SIC	Sea-Ice Concentration
TEP	Transparent Exopolymer Particles
TChla	Total Chlorophyll *a*

https://doi.org/10.5194/egusphere-2025-4190
Preprint. Discussion started: 4 October 2025

Table A2. Volume-weighted mean concentration and standard deviation (STD) of transparent exopolymer particles (TEP) binned for Longhurst Provinces of the upper 30 m ocean depth of the simulated period 2000 to 2019.

Province Code	Mean [µg C L^{-1}]	STD [µg C L^{-1}]	Province Code	Mean [µg C L^{-1}]	STD [µg C L^{-1}]
BPLR	33.43	70.49	INDW	11.18	2.06
ARCT	56.60	90.60	AUSW	12.46	6.78
SARC	50.07	74.69	BERS	40.91	77.17
NADR	18.39	19.18	PSAE	12.52	13.80
GFST	22.51	19.54	PSAW	10.11	11.37
NASW	11.40	7.45	KURO	14.75	14.74
NATR	11.70	2.52	NPPF	21.13	17.03
WTRA	10.95	3.47	NPSW	11.28	5.01
ETRA	14.64	3.19	TASM	18.13	12.11
SATL	13.99	7.30	SPSG	12.19	6.37
NECS	32.82	35.12	NPTG	13.04	4.48
CNRY	18.55	11.13	PNEC	10.93	2.56
GUIN	13.60	3.06	PEQD	12.80	4.16
GUIA	10.60	2.03	WARM	9.18	1.45
NWCS	44.67	48.24	ARCH	10.49	2.95
MEDI	18.29	11.41	ALSK	26.09	34.08
CARB	10.93	3.35	CCAL	24.33	17.75
NASE	17.17	10.62	CAMR	12.81	5.28
BRAZ	18.63	9.94	CHIL	9.97	9.10
FKLD	19.48	19.74	CHIN	26.43	20.71
BENG	18.53	8.39	SUND	10.02	1.96
MONS	10.59	1.63	AUSE	12.38	5.49
ISSG	13.30	6.36	NEWZ	17.51	16.19
EAFR	12.81	4.73	SSTC	14.44	12.86
REDS	11.03	2.34	SANT	7.22	9.89
ARAB	12.39	2.61	ANTA	16.15	29.95
INDE	9.10	2.22	APLR	22.22	39.82

https://doi.org/10.5194/egusphere-2025-4190
Preprint. Discussion started: 4 October 2025

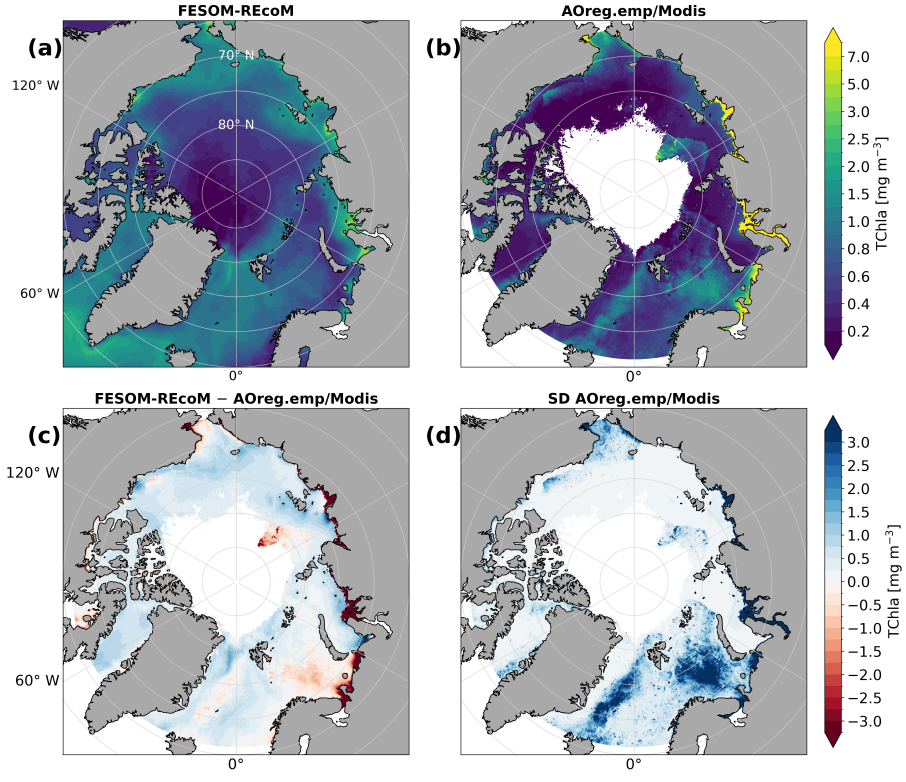

Figure A1. Maps of surface total Chlorophyll *a* (TChla) of FESOM2.1–REcoM3 (panel a), TChla of processed Modis/Aqua data of the Arctic Ocean product AOreg.emp of Lewis and Arrigo (2020) (panel b), the difference of AOreg.emp to the model results (panel c), and the standard deviation of AOreg.emp (panel d). Data is presented as average of May to September over the years 2003 to 2019. AOreg.emp data does not cover the central Arctic Ocean.

https://doi.org/10.5194/egusphere-2025-4190
Preprint. Discussion started: 4 October 2025

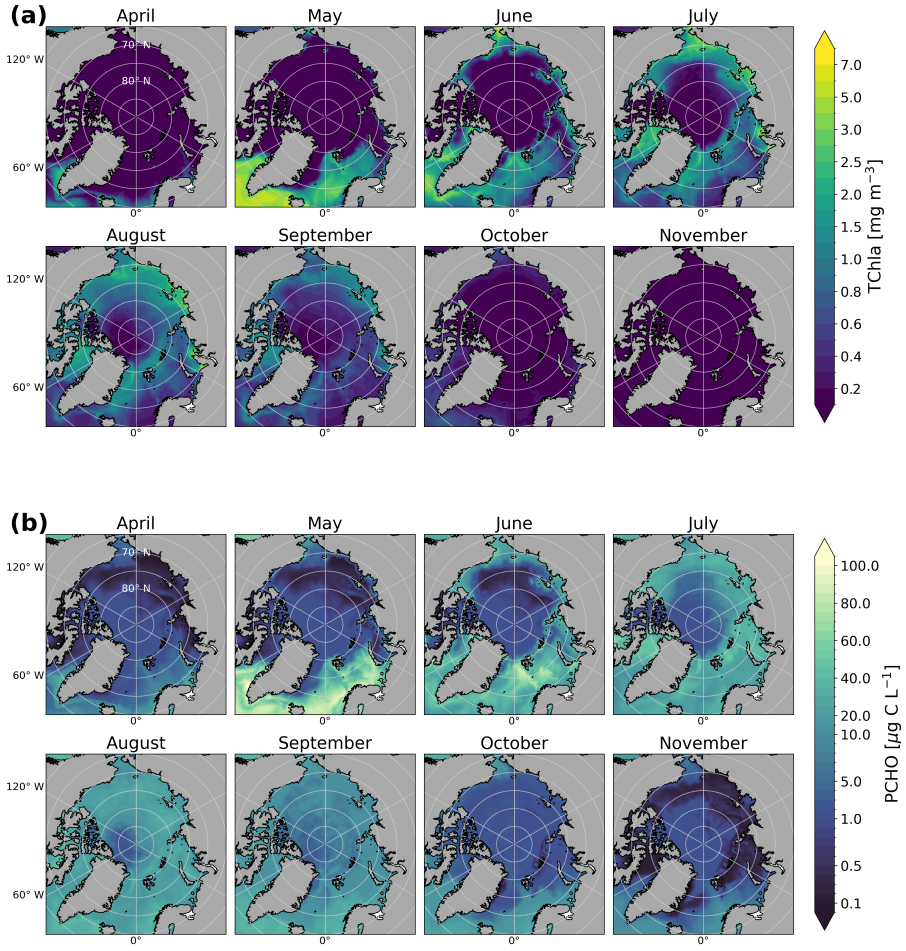

Figure A2. Climatological maps of simulated total Chlorophyll *a* (TChla, panel group a) concentration and simulated dissolved acidic polysaccharide (PCHO, panel group b) concentration as volume-weighted mean of 0–30 m of 2000 to 2019.

https://doi.org/10.5194/egusphere-2025-4190
Preprint. Discussion started: 4 October 2025

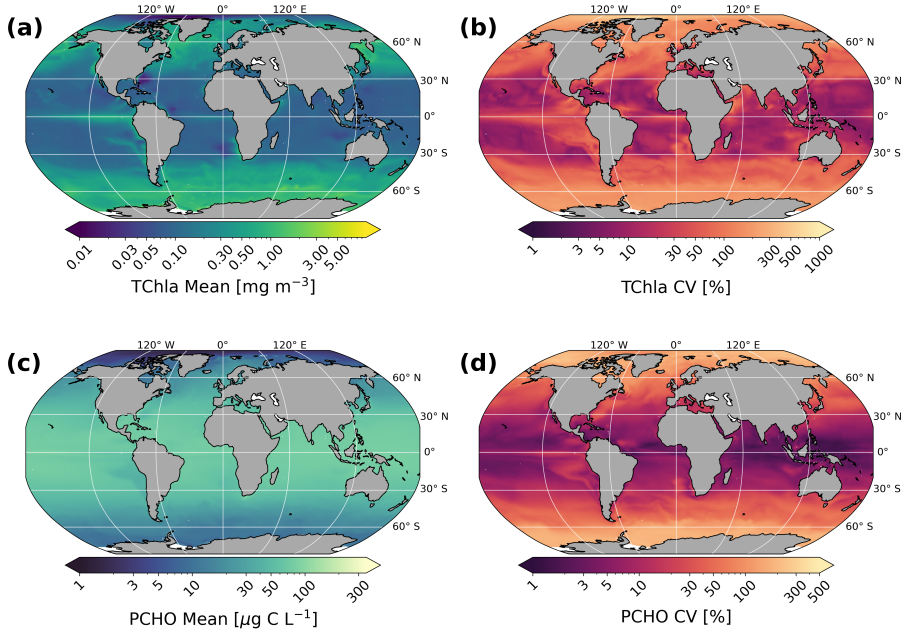

Figure A3. Global maps of simulated total Chlorophyll *a* (TChla, upper row) concentration (panel a), its coefficient of variation (CV, panel b), simulated dissolved acidic polysaccharide (PCHO, lower row) concentration as volume-weighted mean (panel c) and its coefficient of variation (panel d). Mean concentrations and their CV are computed based on volume-weighted means of 0–30 m of 2000 to 2019.

https://doi.org/10.5194/egusphere-2025-4190
Preprint. Discussion started: 4 October 2025

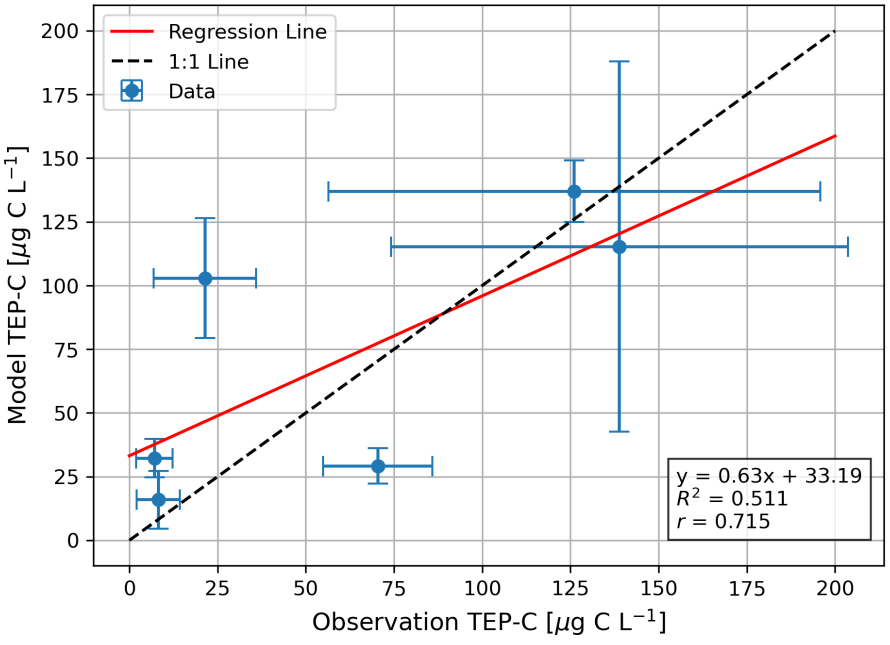

Figure A4. Correlation of the carbon concentration of transparent exopolymer particles (TEP) of observational campaigns and of the simulation. The horizontal error bars represent the standard deviation of the observations, and the vertical ones the standard deviation of the simulation. Model results are volume-weighted and averaged corresponding to the depth range, area, and month of observations, i.e. of Wurl et al. (2011, W2011), Engel et al. (2020, E2020), von Jackowski et al. (2020, vJ2020), and Yamada et al. (2015, Y2015). See also Tab. 5 for background information on the time period, region, and depth range of the simulation and observations. A linear regression is displayed as red line, resulting in a correlation coefficient of 0.71 ($p = 0.11$). Data points for TEP concentrations below 1 µg C L^{-1} have been excluded.

https://doi.org/10.5194/egusphere-2025-4190
Preprint. Discussion started: 4 October 2025

Author contributions. AB, JH, SL, ST, and MZ conceptualized the study. MZ implemented the TEP parametrization into FESOM2.1–REcoM3 and carried out the model simulation as well as the analysis. LO, ST, ÖG, and SL provided support during the setup of the model and during the analysis. SZ and MvP provided the in situ measurement data on dissolved and particulate combined carbohydrates in surface seawater. MZ retrieved and processed the remote sensing dataset on TChla of the Copernicus Marine Environment Monitoring Service. MZ created all figures and wrote the manuscript, to which all authors contributed valuable comments and suggestions.

Competing interests. The authors declare no competing interests.

Acknowledgements. We gratefully acknowledge the funding by the Deutsche Forschungsgemeinschaft (DFG, German Research Foundation) – Projektnummer 268020496 – TRR 172, within the Transregional Collaborative Research Center "ArctiC Amplification: Climate Relevant Atmospheric and SurfaCe Processes, and Feedback Mechanisms (AC)3 in subprojects B04, C03, D02. The contribution of SNL and AB was additionally funded by EU Horizon 2020 Coordination and Support Action (CSA) project KEPLER 2020-SPACE-2018-2020, grant agreement No. 821984. The contribution of SNL was partly made in the framework of the state assignment of SIO RAS (theme FMWE-2024-0028) before February 2022. LO was funded by the European Union's Horizon 2020 research and innovation programm (project COMFORT; 'Our common future ocean in the Earth system–quantifying coupled cycles of carbon, oxygen, and nutrients for determining and achieving safe operating spaces with respect to tipping points'; grant number 820989), by the Federal Ministry of Education and Research of Germany (BMBF) through the project 'nuArctic' (grant number 03F0918A). JH, LO and OG were supported by the Initiative and Networking Fund of the Helmholtz Association (Helmholtz Young Investigator Group Marine Carbon and Ecosystem Feedbacks in the Earth System [MarESys], grant number VH-NG-1301). Furthermore, the authors gratefully acknowledge the computing time granted by the Resource Allocation Board and provided on the supercomputer Lise and Emmy at NHR@ZIB and NHR@Göttingen as part of the NHR infrastructure. The calculations for this research were conducted with computing resources under the project hbk00084. We thank J. Chylik, E. Farrell, R. McPherson, R. Mole, and A. Murray for providing suggestions for the manuscript. Grammarly was used to check for grammar and spelling (grammarly.com). We thank O. Wurl, A. Engel and others for publishing valuable data on ocean surface concentration of various parameters, which helped to adjust and evaluate the model. We want to highlight multiple fruitful discussions within the Plankton Ecology and Biogeochemistry in a Changing Arctic Ocean (PEBCAO) team on this study. We acknowledge the efforts of NASA, ESA, EUMETSAT, and CMEMS for the ocean color products.

https://doi.org/10.5194/egusphere-2025-4190
Preprint. Discussion started: 4 October 2025

References

Alldredge, A. L. and Crocker, K. M.: Why Do Sinking Mucilage Aggregates Accumulate in the Water Column?, Science of The Total Environment, 165, 15–22, https://doi.org/10.1016/0048-9697(95)04539-D, 1995.

Alldredge, A. L., Passow, U., and Logan, B. E.: The Abundance and Significance of a Class of Large, Transparent Organic Particles in the Ocean, Deep Sea Research Part I: Oceanographic Research Papers, 40, 1131–1140, https://doi.org/10.1016/0967-0637(93)90129-Q, 1993.

Álvarez, E., Thoms, S., Bracher, A., Liu, Y., and Völker, C.: Modeling Photoprotection at Global Scale: The Relative Role of Nonphotosynthetic Pigments, Physiological State, and Species Composition, Global Biogeochemical Cycles, 33, https://doi.org/10.1029/2018GB006101, 2019.

Arnosti, C., Wietz, M., Brinkhoff, T., Hehemann, J.-H., Probandt, D., Zeugner, L., and Amann, R.: The Biogeochemistry of Marine Polysaccharides: Sources, Inventories, and Bacterial Drivers of the Carbohydrate Cycle, Annual Review of Marine Science, 13, 81–108, https://doi.org/10.1146/annurev-marine-032020-012810, 2021.

Arrigo, K. R., Perovich, D. K., Pickart, R. S., Brown, Z. W., van Dijken, G. L., Lowry, K. E., Mills, M. M., Palmer, M. A., Balch, W. M., Bates, N. R., et al.: Phytoplankton Blooms beneath the Sea Ice in the Chukchi Sea, Deep Sea Research Part II: Topical Studies in Oceanography, 105, 1–16, 2014.

Aumont, O., Ethé, C., Tagliabue, A., Bopp, L., and Gehlen, M.: PISCES-v2: An Ocean Biogeochemical Model for Carbon and Ecosystem Studies, Geosci. Model Dev., 8, 2465–2513, https://doi.org/10.5194/gmd-8-2465-2015, 2015.

Azetsu-Scott, K. and Passow, U.: Ascending Marine Particles: Significance of Transparent Exopolymer Particles (TEP) in the Upper Ocean, Limnology and Oceanography, 49, 741–748, https://doi.org/10.4319/lo.2004.49.3.0741, 2004.

Burrows, S. M., Ogunro, O., Frossard, A. A., Russell, L. M., Rasch, P. J., and Elliott, S. M.: A Physically Based Framework for Modeling the Organic Fractionation of Sea Spray Aerosol from Bubble Film Langmuir Equilibria, Atmos. Chem. Phys., 14, 13 601–13 629, https://doi.org/10.5194/acp-14-13601-2014, 2014.

Castellani, G., Losch, M., Lange, B. A., and Flores, H.: Modeling Arctic Sea-Ice Algae: Physical Drivers of Spatial Distribution and Algae Phenology, Journal of Geophysical Research: Oceans, 122, 7466–7487, https://doi.org/10.1002/2017JC012828, 2017.

Chajwa, R., Flaum, E., Bidle, K. D., Van Mooy, B., and Prakash, M.: Hidden Comet Tails of Marine Snow Impede Ocean-Based Carbon Sequestration, Science, 386, eadl5767, https://doi.org/10.1126/science.adl5767, 2024.

Cherkasheva, A., Bracher, A., Melsheimer, C., Köberle, C., Gerdes, R., Nöthig, E.-M., Bauerfeind, E., and Boetius, A.: Influence of the Physical Environment on Polar Phytoplankton Blooms: A Case Study in the Fram Strait, Journal of Marine Systems, 132, 196–207, https://doi.org/10.1016/j.jmarsys.2013.11.008, 2014.

Chin, W.-C., Orellana, M. V., Quesada, I., and Verdugo, P.: Secretion in Unicellular Marine Phytoplankton: Demonstration of Regulated Exocytosis in Phaeocystis Globosa, Plant and Cell Physiology, 45, 535–542, https://doi.org/10.1093/pcp/pch062, 2004.

Copernicus Marine Service: Arctic Ocean Colour Plankton Multi-Year L4 Daily Climatology and Monthly Observations, https://doi.org/10.48670/MOI-00293, 2022.

Copernicus Marine Service: Quality Information Document, Tech. rep., Mercator Ocean International, 2023.

Corzo, A., Rodríguez-Gálvez, S., Lubian, L., Sangrá, P., Martínez, A., and Morillo, J. A.: Spatial Distribution of Transparent Exopolymer Particles in the Bransfield Strait, Antarctica, Journal of Plankton Research, 27, 635–646, https://doi.org/10.1093/plankt/fbi038, 2005.

Danilov, S., Sidorenko, D., Wang, Q., and Jung, T.: The Finite-volumE Sea Ice–Ocean Model (FESOM2), Geosci. Model Dev., 10, 765–789, https://doi.org/10.5194/gmd-10-765-2017, 2017.

https://doi.org/10.5194/egusphere-2025-4190
Preprint. Discussion started: 4 October 2025

Discart, V., Bilad, M. R., and Vankelecom, I. F. J.: Critical Evaluation of the Determination Methods for Transparent Exopolymer Particles, Agents of Membrane Fouling, Critical Reviews in Environmental Science and Technology, 45, 167–192, https://doi.org/10.1080/10643389.2013.829982, 2015.

Engel, A.: Determination of Marine Gel Particles, in: Practical Guidelines for the Analysis of Seawater, pp. 125–142, CRC-Press, Boca Raton, USA, ISBN 978-1-4200-7306-5, 2009.

Engel, A. and Händel, N.: A Novel Protocol for Determining the Concentration and Composition of Sugars in Particulate and in High Molecular Weight Dissolved Organic Matter (HMW-DOM) in Seawater, Marine Chemistry, 127, 180–191, https://doi.org/10.1016/j.marchem.2011.09.004, 2011.

Engel, A., Thoms, S., Riebesell, U., Rochelle-Newall, E., and Zondervan, I.: Polysaccharide Aggregation as a Potential Sink of Marine Dissolved Organic Carbon, Nature, 428, 929–932, https://doi.org/10.1038/nature02453, 2004.

Engel, A., Bange, H. W., Cunliffe, M., Burrows, S. M., Friedrichs, G., Galgani, L., Herrmann, H., Hertkorn, N., Johnson, M., Liss, P. S., Quinn, P. K., Schartau, M., Soloviev, A., Stolle, C., Upstill-Goddard, R. C., van Pinxteren, M., and Zäncker, B.: The Ocean's Vital Skin: Toward an Integrated Understanding of the Sea Surface Microlayer, Frontiers in Marine Science, 4, 165, https://doi.org/10.3389/fmars.2017.00165, 2017.

Engel, A., Bracher, A., Dinter, T., Endres, S., Grosse, J., Metfies, K., Peeken, I., Piontek, J., Salter, I., and Nöthig, E.-M.: Inter-Annual Variability of Organic Carbon Concentrations across the Fram Strait (Arctic Ocean) during Summer 2009–2017, Front. Mar. Sci., 6 (187), https://doi.org/doi:10.3389/fmars.2019.00187, 2019.

Engel, A., Endres, S., Galgani, L., and Schartau, M.: Marvelous Marine Microgels: On the Distribution and Impact of Gel-Like Particles in the Oceanic Water-Column, Frontiers in Marine Science, 7, 405, https://doi.org/10.3389/fmars.2020.00405, 2020.

Flanders Marine Institute: Longhurst Provinces, https://www.marineregions.org/, 2009.

Friedlingstein, P., O'Sullivan, M., Jones, M. W., Andrew, R. M., Bakker, D. C. E., Hauck, J., Landschützer, P., Le Quéré, C., Luijkx, I. T., Peters, G. P., Peters, W., Pongratz, J., Schwingshackl, C., Sitch, S., Canadell, J. G., Ciais, P., Jackson, R. B., Alin, S. R., Anthoni, P., Barbero, L., Bates, N. R., Becker, M., Bellouin, N., Decharme, B., Bopp, L., Brasika, I. B. M., Cadule, P., Chamberlain, M. A., Chandra, N., Chau, T.-T.-T., Chevallier, F., Chini, L. P., Cronin, M., Dou, X., Enyo, K., Evans, W., Falk, S., Feely, R. A., Feng, L., Ford, D. J., Gasser, T., Ghattas, J., Gkritzalis, T., Grassi, G., Gregor, L., Gruber, N., Gürses, Ö., Harris, I., Hefner, M., Heinke, J., Houghton, R. A., Hurtt, G. C., Iida, Y., Ilyina, T., Jacobson, A. R., Jain, A., Jarníková, T., Jersild, A., Jiang, F., Jin, Z., Joos, F., Kato, E., Keeling, R. F., Kennedy, D., Klein Goldewijk, K., Knauer, J., Korsbakken, J. I., Körtzinger, A., Lan, X., Lefèvre, N., Li, H., Liu, J., Liu, Z., Ma, L., Marland, G., Mayot, N., McGuire, P. C., McKinley, G. A., Meyer, G., Morgan, E. J., Munro, D. R., Nakaoka, S.-I., Niwa, Y., O'Brien, K. M., Olsen, A., Omar, A. M., Ono, T., Paulsen, M., Pierrot, D., Pocock, K., Poulter, B., Powis, C. M., Rehder, G., Resplandy, L., Robertson, E., Rödenbeck, C., Rosan, T. M., Schwinger, J., Séférian, R., Smallman, T. L., Smith, S. M., Sospedra-Alfonso, R., Sun, Q., Sutton, A. J., Sweeney, C., Takao, S., Tans, P. P., Tian, H., Tilbrook, B., Tsujino, H., Tubiello, F., van der Werf, G. R., van Ooijen, E., Wanninkhof, R., Watanabe, M., Wimart-Rousseau, C., Yang, D., Yang, X., Yuan, W., Yue, X., Zaehle, S., Zeng, J., and Zheng, B.: Global Carbon Budget 2023, Earth Syst. Sci. Data, 15, 5301–5369, https://doi.org/10.5194/essd-15-5301-2023, 2023.

Galgani, L., Piontek, J., and Engel, A.: Biopolymers Form a Gelatinous Microlayer at the Air-Sea Interface When Arctic Sea Ice Melts, Scientific Reports, 6, 29 465, https://doi.org/10.1038/srep29465, 2016.

Gao, Q., Leck, C., Rauschenberg, C., and Matrai, P. A.: On the Chemical Dynamics of Extracellular Polysaccharides in the High Arctic Surface Microlayer, Ocean Sci., 8, 401–418, https://doi.org/10.5194/os-8-401-2012, 2012.

https://doi.org/10.5194/egusphere-2025-4190
Preprint. Discussion started: 4 October 2025

Garcia, HE., Weathers, KW., Paver, CR., Smolyar, I., Boyer, TP., Locarnini, MM., Zweng, MM., Mishonov, AV., Baranova, OK., and Seidov, D.: World Ocean Atlas 2018, Volume 3: Dissolved Oxygen, Apparent Oxygen Utilization, and Dissolved Oxygen Saturation., A. Mishonov Technical Editor, Tech. rep., NOAA Atlas NESDIS, 2019a.

Garcia, HE., Weathers, KW., Paver, CR., Smolyar, I., Boyer, TP., Locarnini, MM., Zweng, MM., Mishonov, AV., Baranova, OK., and Seidov, D.: World Ocean Atlas 2018. Vol. 4: Dissolved Inorganic Nutrients (Phosphate, Nitrate and Nitrate+ Nitrite, Silicate), A. Mishonov Technical Editor, Tech. rep., NOAA Atlas NESDIS, 2019b.

Gehlen, M., Bopp, L., Emprin, N., Aumont, O., Heinze, C., and Ragueneau, O.: Reconciling Surface Ocean Productivity, Export Fluxes and Sediment Composition in a Global Biogeochemical Ocean Model, Biogeosciences, 3, 521–537, https://doi.org/10.5194/bg-3-521-2006, 2006.

Geider, R. J., MacIntyre, H. L., and Kana, T. M.: A Dynamic Regulatory Model of Phytoplanktonic Acclimation to Light, Nutrients, and Temperature, Limnology and Oceanography, 43, 679–694, https://doi.org/10.4319/lo.1998.43.4.0679, 1998.

Goosse, H., Kay, J. E., Armour, K. C., Bodas-Salcedo, A., Chepfer, H., Docquier, D., Jonko, A., Kushner, P. J., Lecomte, O., Massonnet, F., Park, H.-S., Pithan, F., Svensson, G., and Vancoppenolle, M.: Quantifying Climate Feedbacks in Polar Regions, Nature Communications, 9, 1919, https://doi.org/10.1038/s41467-018-04173-0, 2018.

Gürses, Ö., Oziel, L., Karakuş, O., Sidorenko, D., Völker, C., Ye, Y., Zeising, M., Butzin, M., and Hauck, J.: Ocean Biogeochemistry in the Coupled Ocean–Sea Ice–Biogeochemistry Model FESOM2.1–REcoM3, Geosci. Model Dev., 16, 4883–4936, https://doi.org/10.5194/gmd-16-4883-2023, 2023.

Hamacher-Barth, E., Leck, C., and Jansson, K.: Size-Resolved Morphological Properties of the High Arctic Summer Aerosol during ASCOS-2008, Atmos. Chem. Phys., 16, 6577–6593, https://doi.org/10.5194/acp-16-6577-2016, 2016.

Hansell, D., Carlson, C., Repeta, D., and Schlitzer, R.: Dissolved Organic Matter in the Ocean: A Controversy Stimulates New Insights, Oceanography, 22, 202–211, https://doi.org/10.5670/oceanog.2009.109, 2009.

Hansell, D. A. and Orellana, M. V.: Dissolved Organic Matter in the Global Ocean: A Primer, Gels, 7, https://doi.org/10.3390/gels7030128, 2021.

Hansell, D. A., Romera-Castillo, C., and Lopez, C. N.: Dynamics of Dissolved Organic Carbon in the Global Ocean, in: Biogeochemistry of Marine Dissolved Organic Matter (Third Edition), edited by Hansell, D. A. and Carlson, C. A., pp. 769–802, Academic Press, ISBN 978-0-443-13858-4, https://doi.org/10.1016/B978-0-443-13858-4.00004-6, 2024.

Hartmann, M., Adachi, K., Eppers, O., Haas, C., Herber, A., Holzinger, R., Hünerbein, A., Jäkel, E., Jentzsch, C., van Pinxteren, M., Wex, H., Willmes, S., and Stratmann, F.: Wintertime Airborne Measurements of Ice Nucleating Particles in the High Arctic: A Hint to a Marine, Biogenic Source for Ice Nucleating Particles, Geophysical Research Letters, 47, e2020GL087 770, https://doi.org/10.1029/2020GL087770, 2020.

Hauck, J., Völker, C., Wang, T., Hoppema, M., Losch, M., and Wolf-Gladrow, D. A.: Seasonally Different Carbon Flux Changes in the Southern Ocean in Response to the Southern Annular Mode, Global Biogeochemical Cycles, 27, 1236–1245, https://doi.org/10.1002/2013GB004600, 2013.

Hauck, J., Zeising, M., Le Quéré, C., Gruber, N., Bakker, D. C. E., Bopp, L., Chau, T. T. T., Gürses, Ö., Ilyina, T., Landschützer, P., Lenton, A., Resplandy, L., Rödenbeck, C., Schwinger, J., and Séférian, R.: Consistency and Challenges in the Ocean Carbon Sink Estimate for the Global Carbon Budget, Frontiers in Marine Science, 7, 571 720, https://doi.org/10.3389/fmars.2020.571720, 2020.

https://doi.org/10.5194/egusphere-2025-4190
Preprint. Discussion started: 4 October 2025

Heim, B., Abramova, E., Doerffer, R., Günther, F., Hölemann, J., Kraberg, A., Lantuit, H., Loginova, A., Martynov, F., Overduin, P. P., and Wegner, C.: Ocean Colour Remote Sensing in the Southern Laptev Sea: Evaluation and Applications, Biogeosciences, 11, 4191–4210, https://doi.org/10.5194/bg-11-4191-2014, 2014.

Henson, S. A., Laufkötter, C., Leung, S., Giering, S. L. C., Palevsky, H. I., and Cavan, E. L.: Uncertain Response of Ocean Biological Carbon Export in a Changing World, Nature Geoscience, 15, 248–254, https://doi.org/10.1038/s41561-022-00927-0, 2022.

Ickes, L., Porter, G. C. E., Wagner, R., Adams, M. P., Bierbauer, S., Bertram, A. K., Bilde, M., Christiansen, S., Ekman, A. M. L., Gorokhova, E., Höhler, K., Kiselev, A. A., Leck, C., Möhler, O., Murray, B. J., Schiebel, T., Ullrich, R., and Salter, M. E.: The Ice-Nucleating Activity of Arctic Sea Surface Microlayer Samples and Marine Algal Cultures, Atmos. Chem. Phys., 20, 11 089–11 117, https://doi.org/10.5194/acp-20-11089-2020, 2020.

Irish, V. E., Elizondo, P., Chen, J., Chou, C., Charette, J., Lizotte, M., Ladino, L. A., Wilson, T. W., Gosselin, M., Murray, B. J., Polishchuk, E., Abbatt, J. P. D., Miller, L. A., and Bertram, A. K.: Ice-Nucleating Particles in Canadian Arctic Sea-Surface Microlayer and Bulk Seawater, Atmospheric Chemistry and Physics, 17, 10 583–10 595, https://doi.org/10.5194/acp-17-10583-2017, 2017.

Iversen, M. H.: Carbon Export in the Ocean: A Biologist' Perspective, Annual Review of Marine Science, 15, 357–381, https://doi.org/10.1146/annurev-marine-032122-035153, 2023.

Iversen, M. H. and Lampitt, R. S.: Size Does Not Matter after All: No Evidence for a Size-Sinking Relationship for Marine Snow, Progress in Oceanography, 189, 102 445, https://doi.org/10.1016/j.pocean.2020.102445, 2020.

Jokulsdottir, T. and Archer, D.: A Stochastic, Lagrangian Model of Sinking Biogenic Aggregates in the Ocean (SLAMS 1.0): Model Formulation, Validation and Sensitivity, Geoscientific Model Development, 9, 1455–1476, https://doi.org/10.5194/gmd-9-1455-2016, 2016.

Jung, J., Lee, Y., Cho, K.-H., Yang, E. J., and Kang, S.-H.: Spatial Distributions of Riverine and Marine Dissolved Organic Carbon in the Western Arctic Ocean: Results From the 2018 Korean Expedition, Journal of Geophysical Research: Oceans, 127, e2021JC017 718, https://doi.org/10.1029/2021JC017718, 2022.

Karakuş, O., Völker, C., Iversen, M., Hagen, W., Gladrow, D. W., Fach, B., and Hauck, J.: Modeling the Impact of Macrozooplankton on Carbon Export Production in the Southern Ocean, Journal of Geophysical Research: Oceans, n/a, e2021JC017 315, https://doi.org/10.1029/2021JC017315, 2021.

Karakuş, O., Volker, C., Iversen, M., Hagen, W., and Hauck, J.: The Role of Zooplankton Grazing and Nutrient Recycling for Global Ocean Biogeochemistry and Phytoplankton Phenology, Journal of Geophysical Research: Biogeosciences, 127, https://doi.org/10.1029/2022JG006798, 2022.

Krembs, C. and Deming, J. W.: The Role of Exopolymers in Microbial Adaptation to Sea Ice, in: Psychrophiles: From Biodiversity to Biotechnology, pp. 247–264, Springer, 2008.

Kriest, I. and Evans, G. T.: Representing Phytoplankton Aggregates in Biogeochemical Models, Deep Sea Research Part I: Oceanographic Research Papers, 46, 1841–1859, https://doi.org/10.1016/S0967-0637(99)00032-1, 1999.

Kriest, I. and Oschlies, A.: On the Treatment of Particulate Organic Matter Sinking in Large-Scale Models of Marine Biogeochemical Cycles, Biogeosciences, 5, 55–72, https://doi.org/10.5194/bg-5-55-2008, 2008.

Laufkötter, C., Vogt, M., Gruber, N., Aita-Noguchi, M., Aumont, O., Bopp, L., Buitenhuis, E., Doney, S. C., Dunne, J., Hashioka, T., Hauck, J., Hirata, T., John, J., Le Quéré, C., Lima, I. D., Nakano, H., Seferian, R., Totterdell, I., Vichi, M., and Völker, C.: Drivers and Uncertainties of Future Global Marine Primary Production in Marine Ecosystem Models, Biogeosciences, 12, 6955–6984, https://doi.org/10.5194/bg-12-6955-2015, 2015.

https://doi.org/10.5194/egusphere-2025-4190
Preprint. Discussion started: 4 October 2025

Laufkötter, C., Vogt, M., Gruber, N., Aumont, O., Bopp, L., Doney, S. C., Dunne, J. P., Hauck, J., John, J. G., Lima, I. D., Seferian, R., and Völker, C.: Projected Decreases in Future Marine Export Production: The Role of the Carbon Flux through the Upper Ocean Ecosystem, Biogeosciences, 13, 4023–4047, https://doi.org/10.5194/bg-13-4023-2016, 2016.

Lauvset, S. K., Key, R. M., Olsen, A., van Heuven, S., Velo, A., Lin, X., Schirnick, C., Kozyr, A., Tanhua, T., Hoppema, M., Jutterström, S., Steinfeldt, R., Jeansson, E., Ishii, M., Perez, F. F., Suzuki, T., and Watelet, S.: A New Global Interior Ocean Mapped Climatology: The $1^\circ \times 1^\circ$ GLODAP Version 2, Earth Syst. Sci. Data, 8, 325–340, https://doi.org/10.5194/essd-8-325-2016, 2016.

Lawler, M. J., Saltzman, E. S., Karlsson, L., Zieger, P., Salter, M., Baccarini, A., Schmale, J., and Leck, C.: New Insights Into the Composition and Origins of Ultrafine Aerosol in the Summertime High Arctic, Geophysical Research Letters, 48, e2021GL094 395, https://doi.org/10.1029/2021GL094395, 2021.

Leck, C. and Bigg, E. K.: Biogenic Particles in the Surface Microlayer and Overlaying Atmosphere in the Central Arctic Ocean during Summer, Tellus B: Chemical and Physical Meteorology, 57, 305–316, https://doi.org/10.3402/tellusb.v57i4.16546, 2005.

Lennartz, S. T., Keller, D. P., Oschlies, A., Blasius, B., and Dittmar, T.: Mechanisms Underpinning the Net Removal Rates of Dissolved Organic Carbon in the Global Ocean, Global Biogeochemical Cycles, 38, e2023GB007 912, https://doi.org/10.1029/2023GB007912, 2024.

Leon-Marcos, A., Zeising, M., van Pinxteren, M., Zeppenfeld, S., Bracher, A., Barbaro, E., Engel, A., Feltracco, M., Tegen, I., and Heinold, B.: Modelling Emission and Transport of Key Components of Primary Marine Organic Aerosol Using the Global Aerosol–Climate Model ECHAM6.3–HAM2.3, Geosci. Model Dev., 18, 4183–4213, https://doi.org/10.5194/gmd-18-4183-2025, 2025.

Levine, N. M. and DeVries, T.: Modeling DOM from the Ecosystem to Global Scales, in: Biogeochemistry of Marine Dissolved Organic Matter (Third Edition), edited by Hansell, D. A. and Carlson, C. A., pp. 803–820, Academic Press, ISBN 978-0-443-13858-4, https://doi.org/10.1016/B978-0-443-13858-4.00019-8, 2024.

Lewis, K. M. and Arrigo, K. R.: Ocean Color Algorithms for Estimating Chlorophyll a, CDOM Absorption, and Particle Backscattering in the Arctic Ocean, Journal of Geophysical Research: Oceans, 125, e2019JC015 706, https://doi.org/10.1029/2019JC015706, 2020.

Lewis, K. M., van Dijken, G. L., and Arrigo, K. R.: Changes in Phytoplankton Concentration Now Drive Increased Arctic Ocean Primary Production, Science, 369, 198–202, https://doi.org/10.1126/science.aay8380, 2020.

Longhurst, A. R.: Ecological Geography of the Sea, Academic Press, San Diego, 2nd edition edn., ISBN 978-0-12-455521-1, 2006.

Macke, A. and Flores, H.: The Expeditions PS106/1 and 2 of the Research Vessel POLARSTERN to the Arctic Ocean in 2017, https://doi.org/10.2312/BzPM_0719_2018, 2018.

Maerz, J., Six, K. D., Stemmler, I., Ahmerkamp, S., and Ilyina, T.: Microstructure and Composition of Marine Aggregates as Co-Determinants for Vertical Particulate Organic Carbon Transfer in the Global Ocean, Biogeosciences, 17, 1765–1803, https://doi.org/10.5194/bg-17-1765-2020, 2020.

Monterey, G. I. and Levitus, S.: Seasonal Variability of Mixed Layer Depth for the World Ocean, NOAA Atlas NESDIS, 14, 1997.

Mustapha, S. B., , Simon, B., and and Larouche, P.: Evaluation of Ocean Color Algorithms in the Southeastern Beaufort Sea, Canadian Arctic: New Parameterization Using SeaWiFS, MODIS, and MERIS Spectral Bands, Canadian Journal of Remote Sensing, 38, 535–556, https://doi.org/10.5589/m12-045, 2012.

Nissen, C., Timmermann, R., Hoppema, M., Gürses, Ö., and Hauck, J.: Abruptly Attenuated Carbon Sequestration with Weddell Sea Dense Waters by 2100, Nature Communications, 13, 3402, https://doi.org/10.1038/s41467-022-30671-3, 2022.

Nissen, C., Timmermann, R., Hoppema, M., and Hauck, J.: A Regime Shift on Weddell Sea Continental Shelves with Local and Remote Physical and Biogeochemical Implications Is Avoidable in a 2°C Scenario, Journal of Climate, 36, 6613–6630, https://doi.org/10.1175/JCLI-D-22-0926.1, 2023.

https://doi.org/10.5194/egusphere-2025-4190
Preprint. Discussion started: 4 October 2025

Nissen, C., Lovenduski, N. S., Brooks, C. M., Hoppema, M., Timmermann, R., and Hauck, J.: Severe 21st-Century Ocean Acidification in Antarctic Marine Protected Areas, Nature Communications, 15, 259, https://doi.org/10.1038/s41467-023-44438-x, 2024.

Nöthig, E.-M., Ramondenc, S., Haas, A., Hehemann, L., Walter, A., Bracher, A., Lalande, C., Metfies, K., Peeken, I., Bauerfeind, E., and Boetius, A.: Summertime Chlorophyll a and Particulate Organic Carbon Standing Stocks in Surface Waters of the Fram Strait and the Arctic Ocean (1991–2015), Frontiers in Marine Science, 7, 350, https://doi.org/10.3389/fmars.2020.00350, 2020.

Ogawa, H. and Tanoue, E.: Dissolved Organic Matter in Oceanic Waters, Journal of Oceanography, 59, 129–147, https://doi.org/10.1023/A:1025528919771, 2003.

Olli, K., Wassmann, P., Reigstad, M., Ratkova, T. N., Arashkevich, E., Pasternak, A., Matrai, P. A., Knulst, J., Tranvik, L., Klais, R., and Jacobsen, A.: The Fate of Production in the Central Arctic Ocean – Top–down Regulation by Zooplankton Expatriates?, Progress in Oceanography, 72, 84–113, https://doi.org/10.1016/j.pocean.2006.08.002, 2007.

Orellana, M. V., Matrai, P. A., Leck, C., Rauschenberg, C. D., Lee, A. M., and Coz, E.: Marine Microgels as a Source of Cloud Condensation Nuclei in the High Arctic, Proc. Natl. Acad. Sci., 108, 13 612–13 617, https://doi.org/10.1073/pnas.1102457108, 2011.

Oziel, L., Schourup-Kristensen, V., Wekerle, C., and Hauck, J.: The Pan-Arctic Continental Slope as an Intensifying Conveyer Belt for Nutrients in the Central Arctic Ocean (1985–2015), Global Biogeochemical Cycles, 36, e2021GB007 268, https://doi.org/10.1029/2021GB007268, 2022.

Oziel, L., Gürses, Ö., Torres-Valdés, S., Hoppe, C. J. M., Rost, B., Karakuş, O., Danek, C., Koch, B. P., Nissen, C., Koldunov, N., Wang, Q., Völker, C., Iversen, M., Juhls, B., and Hauck, J.: Climate Change and Terrigenous Inputs Decrease the Efficiency of the Future Arctic Ocean's Biological Carbon Pump, Nature Climate Change, https://doi.org/10.1038/s41558-024-02233-6, 2025.

Pakulski, J. D. and Benner, R.: Abundance and Distribution of Carbohydrates in the Ocean, Limnology and Oceanography, 39, 930–940, 1994.

Park, J., Dall'Osto, M., Park, K., Kim, J.-H., Park, J., Park, K.-T., Hwang, C. Y., Jang, G. I., Gim, Y., Kang, S., Park, S., Jin, Y. K., Yum, S. S., Simó, R., and Yoon, Y. J.: Arctic Primary Aerosol Production Strongly Influenced by Riverine Organic Matter, Environmental Science & Technology, 53, 8621–8630, https://doi.org/10.1021/acs.est.9b03399, 2019.

Passow, U.: Transparent Exopolymer Particles (TEP) in Aquatic Environments, Progress in Oceanography, 55, 287–333, https://doi.org/10.1016/S0079-6611(02)00138-6, 2002.

Peralta-Ferriz, C. and Woodgate, R. A.: Seasonal and Interannual Variability of Pan-Arctic Surface Mixed Layer Properties from 1979 to 2012 from Hydrographic Data, and the Dominance of Stratification for Multiyear Mixed Layer Depth Shoaling, Progress in Oceanography, 134, 19–53, https://doi.org/10.1016/j.pocean.2014.12.005, 2015.

Piontek, J., Galgani, L., Nöthig, E.-M., Peeken, I., and Engel, A.: Organic Matter Composition and Heterotrophic Bacterial Activity at Declining Summer Sea Ice in the Central Arctic Ocean, Limnology and Oceanography, 66, S343–S362, https://doi.org/10.1002/lno.11639, 2021.

Porter, G. C. E., Adams, M. P., Brooks, I. M., Ickes, L., Karlsson, L., Leck, C., Salter, M. E., Schmale, J., Siegel, K., Sikora, S. N. F., Tarn, M. D., Vüllers, J., Wernli, H., Zieger, P., Zinke, J., and Murray, B. J.: Highly Active Ice-Nucleating Particles at the Summer North Pole, Journal of Geophysical Research: Atmospheres, 127, e2021JD036 059, https://doi.org/10.1029/2021JD036059, 2022.

Randelhoff, A., Holding, J., Janout, M., Sejr, M. K., Babin, M., Tremblay, J.-É., and Alkire, M. B.: Pan-Arctic Ocean Primary Production Constrained by Turbulent Nitrate Fluxes, Frontiers in Marine Science, 7, 150, https://doi.org/10.3389/fmars.2020.00150, 2020.

Repeta, D. and Aluwihare, L.: Chemical Characterization and Cycling of Dissolved Organic Matter, in: Biogeochemistry of Marine Dissolved Organic Matter, pp. 13–67, Elsevier, ISBN 978-0-443-13858-4, https://doi.org/10.1016/B978-0-443-13858-4.00011-3, 2024.

https://doi.org/10.5194/egusphere-2025-4190
Preprint. Discussion started: 4 October 2025

Robinson, T.-B., Wurl, O., Bahlmann, E., Jürgens, K., and Stolle, C.: Rising Bubbles Enhance the Gelatinous Nature of the Air–Sea Interface, Limnology and Oceanography, 64, 2358–2372, https://doi.org/10.1002/lno.11188, 2019.

Schartau, M., Engel, A., Schröter, J., Thoms, S., Völker, C., and Wolf-Gladrow, D.: Modelling Carbon Overconsumption and the Formation of Extracellular Particulate Organic Carbon, Biogeosciences, 4, 433–454, https://doi.org/10.5194/bg-4-433-2007, 2007.

Schmale, J., Zieger, P., and Ekman, A. M. L.: Aerosols in Current and Future Arctic Climate, Nature Climate Change, 11, 95–105, https://doi.org/10.1038/s41558-020-00969-5, 2021.

Schourup-Kristensen, V., Sidorenko, D., Wolf-Gladrow, D. A., and Völker, C.: A Skill Assessment of the Biogeochemical Model REcoM2 Coupled to the Finite Element Sea Ice–Ocean Model (FESOM 1.3), Geoscientific Model Development, 7, 2769–2802, https://doi.org/10.5194/gmd-7-2769-2014, 2014.

Schourup-Kristensen, V., Wekerle, C., Wolf-Gladrow, D. A., and Völker, C.: Arctic Ocean Biogeochemistry in the High Resolution FESOM 1.4-REcoM2 Model, Progress in Oceanography, 168, 65–81, https://doi.org/10.1016/j.pocean.2018.09.006, 2018.

Schourup-Kristensen, V., Wekerle, C., Danilov, S., and Völker, C.: Seasonality of Mesoscale Phytoplankton Control in Eastern Fram Strait, Journal of Geophysical Research: Oceans, 126, e2021JC017 279, https://doi.org/10.1029/2021JC017279, 2021.

Seegers, B. N., Stumpf, R. P., Schaeffer, B. A., Loftin, K. A., and Werdell, P. J.: Performance Metrics for the Assessment of Satellite Data Products: An Ocean Color Case Study, Optics Express, 26, 7404, https://doi.org/10.1364/OE.26.007404, 2018.

Seifert, M., Nissen, C., Rost, B., and Hauck, J.: Cascading Effects Augment the Direct Impact of CO2 on Phytoplankton Growth in a Biogeochemical Model, Elementa: Science of the Anthropocene, 10, 00 104, https://doi.org/10.1525/elementa.2021.00104, 2022.

Semmler, T., Danilov, S., Gierz, P., Goessling, H. F., Hegewald, J., Hinrichs, C., Koldunov, N., Khosravi, N., Mu, L., Rackow, T., Sein, D. V., Sidorenko, D., Wang, Q., and Jung, T.: Simulations for CMIP6 With the AWI Climate Model AWI-CM-1-1, Journal of Advances in Modeling Earth Systems, 12, e2019MS002 009, https://doi.org/10.1029/2019MS002009, 2020.

Steele, D. J., Franklin, D. J., and Underwood, G. J.: Protection of Cells from Salinity Stress by Extracellular Polymeric Substances in Diatom Biofilms, Biofouling, 30, 987–998, https://doi.org/10.1080/08927014.2014.960859, 2014.

Steele, M., Morley, R., and Ermold, W.: PHC: A Global Ocean Hydrography with a High-Quality Arctic Ocean, Journal of Climate, 14, 2079–2087, https://doi.org/10.1175/1520-0442(2001)014<2079:PAGOHW>2.0.CO;2, 2001.

Streffing, J., Sidorenko, D., Semmler, T., Zampieri, L., Scholz, P., Andrés-Martínez, M., Koldunov, N., Rackow, T., Kjellsson, J., Goessling, H., Athanase, M., Wang, Q., Hegewald, J., Sein, D. V., Mu, L., Fladrich, U., Barbi, D., Gierz, P., Danilov, S., Juricke, S., Lohmann, G., and Jung, T.: AWI-CM3 Coupled Climate Model: Description and Evaluation Experiments for a Prototype Post-CMIP6 Model, Geosci. Model Dev., 15, 6399–6427, https://doi.org/10.5194/gmd-15-6399-2022, 2022.

Tagliabue, A., Aumont, O., DeAth, R., Dunne, J. P., Dutkiewicz, S., Galbraith, E., Misumi, K., Moore, J. K., Ridgwell, A., Sherman, E., Stock, C., Vichi, M., Völker, C., and Yool, A.: How Well Do Global Ocean Biogeochemistry Models Simulate Dissolved Iron Distributions?, Global Biogeochemical Cycles, 30, 149–174, https://doi.org/10.1002/2015GB005289, 2016.

Taylor, P. C., Boeke, R. C., Boisvert, L. N., Feldl, N., Henry, M., Huang, Y., Langen, P. L., Liu, W., Pithan, F., Sejas, S. A., and Tan, I.: Process Drivers, Inter-Model Spread, and the Path Forward: A Review of Amplified Arctic Warming, Frontiers in Earth Science, 9, https://doi.org/10.3389/feart.2021.758361, 2022.

Terhaar, J., Lauerwald, R., Regnier, P., Gruber, N., and Bopp, L.: Around One Third of Current Arctic Ocean Primary Production Sustained by Rivers and Coastal Erosion, Nature Communications, 12, 169, https://doi.org/10.1038/s41467-020-20470-z, 2021.

Thornton, D. C.: Dissolved Organic Matter (DOM) Release by Phytoplankton in the Contemporary and Future Ocean, European Journal of Phycology, 49, 20–46, https://doi.org/10.1080/09670262.2013.875596, 2014.

https://doi.org/10.5194/egusphere-2025-4190
Preprint. Discussion started: 4 October 2025

Toggweiler, J. R.: Carbon Overconsumption, Nature, 363, 210–211, https://doi.org/10.1038/363210a0, 1993.

Tsujino, H., Urakawa, S., Nakano, H., Small, R. J., Kim, W. M., Yeager, S. G., Danabasoglu, G., Suzuki, T., Bamber, J. L., Bentsen, M., Böning, C. W., Bozec, A., Chassignet, E. P., Curchitser, E., Boeira Dias, F., Durack, P. J., Griffies, S. M., Harada, Y., Ilicak, M., Josey, S. A., Kobayashi, C., Kobayashi, S., Komuro, Y., Large, W. G., Le Sommer, J., Marsland, S. J., Masina, S., Scheinert, M., Tomita, H., Valdivieso, M., and Yamazaki, D.: JRA-55 Based Surface Dataset for Driving Ocean–Sea-Ice Models (JRA55-do), Ocean Modelling, 130, 79–139, https://doi.org/10.1016/j.ocemod.2018.07.002, 2018.

van Pinxteren, M., Robinson, T.-B., Zeppenfeld, S., Gong, X., Bahlmann, E., Fomba, K. W., Triesch, N., Stratmann, F., Wurl, O., Engel, A., Wex, H., and Herrmann, H.: High Number Concentrations of Transparent Exopolymer Particles in Ambient Aerosol Particles and Cloud Water – a Case Study at the Tropical Atlantic Ocean, Atmos. Chem. Phys., 22, 5725–5742, https://doi.org/10.5194/acp-22-5725-2022, 2022.

Verdugo, P.: Marine Biopolymer Dynamics, Gel Formation, and Carbon Cycling in the Ocean, Gels, 7, https://doi.org/10.3390/gels7030136, 2021.

Verdugo, P., Alldredge, A. L., Azam, F., Kirchman, D. L., Passow, U., and Santschi, P. H.: The Oceanic Gel Phase: A Bridge in the DOM–POM Continuum, Marine Chemistry, 92, 67–85, https://doi.org/10.1016/j.marchem.2004.06.017, 2004.

von Appen, W.-J., Waite, A. M., Bergmann, M., Bienhold, C., Boebel, O., Bracher, A., Cisewski, B., Hagemann, J., Hoppema, M., Iversen, M. H., Konrad, C., Krumpen, T., Lochthofen, N., Metfies, K., Niehoff, B., Nöthig, E.-M., Purser, A., Salter, I., Schaber, M., Scholz, D., Soltwedel, T., Torres-Valdes, S., Wekerle, C., Wenzhöfer, F., Wietz, M., and Boetius, A.: Sea-Ice Derived Meltwater Stratification Slows the Biological Carbon Pump: Results from Continuous Observations, Nature Communications, 12, 7309, https://doi.org/10.1038/s41467-021-26943-z, 2021.

von Jackowski, A., Grosse, J., Nöthig, E.-M., and Engel, A.: Dynamics of Organic Matter and Bacterial Activity in the Fram Strait during Summer and Autumn, Philosophical Transactions of the Royal Society A: Mathematical, Physical and Engineering Sciences, 378, 20190 366, https://doi.org/10.1098/rsta.2019.0366, 2020.

Von Smoluchowski, M.: Versuch Einer Mathematischen Theorie Der Koagulationskinetik Kolloider Lösungen, Zeitschrift für Physikalische Chemie, 92, 129–168, 1917.

Waite, A. M., Thompson, P. A., and Harrison, P. J.: Does Energy Control the Sinking Rates of Marine Diatoms?, Limnology and Oceanography, 37, 468–477, https://doi.org/10.4319/lo.1992.37.3.0468, 1992.

Wang, Q., Danilov, S., Jung, T., Kaleschke, L., and Wernecke, A.: Sea Ice Leads in the Arctic Ocean: Model Assessment, Interannual Variability and Trends, Geophysical Research Letters, 43, 7019–7027, https://doi.org/10.1002/2016GL068696, 2016.

Wang, Q., Wekerle, C., Danilov, S., Wang, X., and Jung, T.: A 4.5 Km Resolution Arctic Ocean Simulation with the Global Multi-Resolution Model FESOM 1.4, Geoscientific Model Development, 11, 1229–1255, https://doi.org/10.5194/gmd-11-1229-2018, 2018.

Wekerle, C., Wang, Q., Danilov, S., Schourup-Kristensen, V., von Appen, W.-J., and Jung, T.: Atlantic Water in the Nordic Seas: Locally Eddy-Permitting Ocean Simulation in a Global Setup, Journal of Geophysical Research: Oceans, 122, 914–940, https://doi.org/10.1002/2016JC012121, 2017.

Wendisch, M., Macke, A., Ehrlich, A., Lüpkes, C., Mech, M., Chechin, D., Dethloff, K., Velasco, C. B., Bozem, H., Brückner, M., Clemen, H.-C., Crewell, S., Donth, T., Dupuy, R., Ebell, K., Egerer, U., Engelmann, R., Engler, C., Eppers, O., Gehrmann, M., Gong, X., Gottschalk, M., Gourbeyre, C., Griesche, H., Hartmann, J., Hartmann, M., Heinold, B., Herber, A., Herrmann, H., Heygster, G., Hoor, P., Jafariserajehlou, S., Jäkel, E., Järvinen, E., Jourdan, O., Kästner, U., Kecorius, S., Knudsen, E. M., Köllner, F., Kretzschmar, J., Lelli, L., Leroy, D., Maturilli, M., Mei, L., Mertes, S., Mioche, G., Neuber, R., Nicolaus, M., Nomokonova, T., Notholt, J., Palm, M., van Pinx-

https://doi.org/10.5194/egusphere-2025-4190
Preprint. Discussion started: 4 October 2025

teren, M., Quaas, J., Richter, P., Ruiz-Donoso, E., Schäfer, M., Schmieder, K., Schnaiter, M., Schneider, J., Schwarzenböck, A., Seifert, P., Shupe, M. D., Siebert, H., Spreen, G., Stapf, J., Stratmann, F., Vogl, T., Welti, A., Wex, H., Wiedensohler, A., Zanatta, M., and Zeppenfeld, S.: The Arctic Cloud Puzzle: Using ACLOUD/PASCAL Multiplatform Observations to Unravel the Role of Clouds and Aerosol Particles in Arctic Amplification, Bulletin of the American Meteorological Society, 100, 841–871, https://doi.org/10.1175/BAMS-D-18-0072.1, 2019.

Wilson, J. D., Andrews, O., Katavouta, A., de Melo Viríssimo, F., Death, R. M., Adloff, M., Baker, C. A., Blackledge, B., Goldsworth, F. W., Kennedy-Asser, A. T., Liu, Q., Sieradzan, K. R., Vosper, E., and Ying, R.: The Biological Carbon Pump in CMIP6 Models: 21st Century Trends and Uncertainties, Proceedings of the National Academy of Sciences, 119, e2204369 119, https://doi.org/10.1073/pnas.2204369119, 2022.

Wilson, T. W., Ladino, L. A., Alpert, P. A., Breckels, M. N., Brooks, I. M., Browse, J., Burrows, S. M., Carslaw, K. S., Huffman, J. A., Judd, C., et al.: A Marine Biogenic Source of Atmospheric Ice-Nucleating Particles, Nature, 525, 234–238, https://doi.org/10.1038/nature14986, 2015.

Wurl, O. and Cunliffe, M.: Transparent Exopolymeric Particles: An Important EPS Component in Seawater, in: The Perfect Slime: Microbial Extracellular Polymeric Substances (EPS), pp. 249–267, IWA publishing, London, ISBN 1-78040-741-6, 2017.

Wurl, O., Miller, L., and Vagle, S.: Production and Fate of Transparent Exopolymer Particles in the Ocean, Journal of Geophysical Research: Oceans, 116, https://doi.org/10.1029/2011JC007342, 2011.

Xi, H., Losa, S. N., Mangin, A., Garnesson, P., Bretagnon, M., Demaria, J., Soppa, M. A., Hembise Fanton d'Andon, O., and Bracher, A.: Global Chlorophyll a Concentrations of Phytoplankton Functional Types With Detailed Uncertainty Assessment Using Multisensor Ocean Color and Sea Surface Temperature Satellite Products, Journal of Geophysical Research: Oceans, 126, e2020JC017 127, https://doi.org/10.1029/2020JC017127, 2021.

Yamada, Y., Fukuda, H., Uchimiya, M., Motegi, C., Nishino, S., Kikuchi, T., and Nagata, T.: Localized Accumulation and a Shelf-Basin Gradient of Particles in the Chukchi Sea and Canada Basin, Western Arctic, Journal of Geophysical Research: Oceans, 120, 4638–4653, https://doi.org/10.1002/2015JC010794, 2015.

Zamanillo, M., Ortega-Retuerta, E., Nunes, S., Rodríguez-Ros, P., Dall'Osto, M., Estrada, M., Montserrat Sala, M., and Simó, R.: Main Drivers of Transparent Exopolymer Particle Distribution across the Surface Atlantic Ocean, Biogeosciences, 16, 733–749, https://doi.org/10.5194/bg-16-733-2019, 2019.

Zampieri, L., Kauker, F., Fröhle, J., Sumata, H., Hunke, E. C., and Goessling, H. F.: Impact of Sea-Ice Model Complexity on the Performance of an Unstructured-Mesh Sea-Ice/Ocean Model under Different Atmospheric Forcings, Journal of Advances in Modeling Earth Systems, 13, e2020MS002 438, https://doi.org/10.1029/2020MS002438, 2021.

Zeising, M., Oziel, L., Gürses, Ö., Hauck, J., Losa, S., Thoms, S., Völker, C., and Bracher, A.: Curated Model Results of TEP Simulation in FESOM2.1-REcoM3, https://doi.org/10.5281/zenodo.15174190, 2025.

Zeppenfeld, S., van Pinxteren, M., Engel, A., and Herrmann, H.: A Protocol for Quantifying Mono- and Polysaccharides in Seawater and Related Saline Matrices by Electro-Dialysis (ED) – Combined with HPAEC-PAD, Ocean Science, 16, 817–830, https://doi.org/10.5194/os-16-817-2020, 2020.

Zeppenfeld, S., Van Pinxteren, M., Van Pinxteren, D., Wex, H., Berdalet, E., Vaqué, D., Dall'Osto, M., and Herrmann, H.: Aerosol Marine Primary Carbohydrates and Atmospheric Transformation in the Western Antarctic Peninsula, ACS Earth and Space Chemistry, 5, 1032–1047, https://doi.org/10.1021/acsearthspacechem.0c00351, 2021.

https://doi.org/10.5194/egusphere-2025-4190
Preprint. Discussion started: 4 October 2025

Zeppenfeld, S., Bracher, A., Wiegmann, S., Zeising, M., Fuchs, S., van Pinxteren, M., and Herrmann, H.: Dissolved and Particulate Combined Carbohydrates, pH, Inorganic Ions, CDOM and Particulate Absorption of SML and Bulk Water in Arctic Surface Seawater and Melt Ponds, https://doi.org/10.1594/PANGAEA.961004, 2023a.

995 Zeppenfeld, S., van Pinxteren, M., Hartmann, M., Zeising, M., Bracher, A., and Herrmann, H.: Marine Carbohydrates in Arctic Aerosol Particles and Fog – Diversity of Oceanic Sources and Atmospheric Transformations, Atmos. Chem. Phys., 23, 15 561–15 587, https://doi.org/10.5194/acp-23-15561-2023, 2023b.

Zhao, X., Liu, X., Burrows, S. M., and Shi, Y.: Effects of Marine Organic Aerosols as Sources of Immersion-Mode Ice-Nucleating Particles on High-Latitude Mixed-Phase Clouds, Atmos. Chem. Phys., 21, 2305–2327, https://doi.org/10.5194/acp-21-2305-2021, 2021.

1000 Zhou, J., Mopper, K., and Passow, U.: The Role of Surface-Active Carbohydrates in the Formation of Transparent Exopolymer Particles by Bubble Adsorption of Seawater, Limnology and Oceanography, 43, 1860–1871, https://doi.org/10.4319/lo.1998.43.8.1860, 1998.

Ziff, R. M. and Stell, G.: Kinetics of Polymer Gelation, The Journal of Chemical Physics, 73, 3492–3499, https://doi.org/10.1063/1.440502, 1980.